

AN INVESTIGATION OF BOND FORMATION BETWEEN  
ALUMINA SINGLE CRYSTALS AND NICKEL ALLOYS

by

JOHN FRANK CLARKE

A THESIS SUBMITTED IN PARTIAL FULFILMENT OF  
THE REQUIREMENTS FOR THE DEGREE OF  
MASTER OF APPLIED SCIENCE

in the Department  
of  
MINING AND METALLURGY

We accept this thesis as conforming to the  
standard required from candidates for the  
degree of MASTER OF APPLIED SCIENCE.

Members of the Department of  
Mining and Metallurgy

THE UNIVERSITY OF BRITISH COLUMBIA

August, 1959

## ABSTRACT

An investigation was conducted on the mechanisms of bond formation between alloys of nickel and single crystals of alumina. Nickel-titanium, nickel-chromium, and nickel-zirconium powder mixtures were cleaned with purified hydrogen gas at 800°C and were individually melted under vacuum ( $10^{-5}$  m.m. of Hg) in contact with alumina. Interfacial energy measurements at 1500°C were made by the sessile-drop method. The bond surfaces were examined by X-ray fluorescence and X-ray diffraction techniques.

The bond formation in all cases appeared to involve two basic mechanisms - metal solute segregation and interfacial reaction. By interfacial measurements and X-ray fluorescence analyses, the solute atoms, titanium and chromium, were shown to be selectively adsorbed at the metal-ceramic interface. Interfacial reaction products were detected by X-ray diffraction methods. The adsorbed titanium reacted with the alumina to produce an interfacial layer of alpha titanium sesqui oxide ( $\alpha\text{-Ti}_2\text{O}_3$ ). Adsorbed chromium similarly reacted with the alumina to form an interfacial compound. However, this compound could not be identified. With nickel-zirconium alloys, the violence of the reaction between zirconium and alumina made experimental measurements impossible.

In presenting this thesis in partial fulfilment of the requirements for an advanced degree at the University of British Columbia, I agree that the Library shall make it freely available for reference and study. I further agree that permission for extensive copying of this thesis for scholarly purposes may be granted by the Head of my Department or by his representatives. It is understood that copying or publication of this thesis for financial gain shall not be allowed without my written permission.

Department of Mining and Metallurgy

The University of British Columbia,  
Vancouver 8, Canada.

Date September 3, 1959.

### ACKNOWLEDGEMENT

The author is indebted to Mr. W.M. Armstrong for his supervision and encouragement, and to Mr. R. Butters for his technical advice and assistance. The invaluable assistance given by Dr. R.M. Thompson in interpreting X-ray data is also gratefully acknowledged.

The work was financed by Research Grant 7510-32 provided by the Defence Research Board of Canada and a Scholarship provided by the University of British Columbia.

## TABLE OF CONTENTS

	<u>Page</u>
I. INTRODUCTION . . . . .	1
A. General Purpose and Scope . . . . .	1
B. Previous Investigations . . . . .	4
C. Specific Aims of the Present Investigation . . . . .	10
II. EXPERIMENTAL . . . . .	12
A. Materials . . . . .	12
1. Aluminum oxide . . . . .	12
2. Metals . . . . .	13
B. Apparatus . . . . .	15
1. Furnace . . . . .	17
2. Vacuum system . . . . .	18
3. Optical system . . . . .	19
C. Preparation of Materials . . . . .	20
D. Experimental Procedure . . . . .	24
1. Sessile-drop experiments . . . . .	24
2. X-ray fluorescence examinations . . . . .	25
3. X-ray diffraction investigations . . . . .	25
III. EXPERIMENTAL RESULTS AND CALCULATIONS . . . . .	27
A. Wetting Results . . . . .	27
B. X-ray Data . . . . .	32
1. X-ray fluorescence analyses . . . . .	32
2. Debye-Scherrer Powder Patterns . . . . .	35
C. Thermodynamic Calculations . . . . .	37

(Continued ...)

Table of Contents (continued)

	<u>Page</u>
IV. DISCUSSION AND CONCLUSIONS . . . . .	39
A. Discussion of Results . . . . .	39
B. Conclusions . . . . .	43
V. RECOMMENDATIONS FOR FURTHER WORK . . . . .	46
VI. APPENDICES . . . . .	47
VII. BIBLIOGRAPHY . . . . .	60

## FIGURES

<u>No.</u>	<u>Page</u>
1. Surface tension forces acting on a sessile drop . . . . .	3
2. Graphs reproduced from the work by Allen and Kingery, and Kurkjian and Kingery . . . . .	7
3. A phase diagram for the Cr <sub>2</sub> O <sub>3</sub> system . . . . .	9
4. Pictorial representation of sapphire lattice. <sup>24</sup> . . . . .	13
5. The apparatus assembly of the induction furnace, vacuum system and optical system . . . . .	15
6. Assembly drawing of the apparatus . . . . .	16
7. Molybdenum heating elements (dismantled) of the induction furnace . . . . .	17
8. (a) Rough-polished surface of sapphire rod; (b) Finished surface of sapphire rod; (c) Finished surface of sintered oxide. Magnification 1000x . . . . .	21
9. Cross-sectional view of a specimen showing shape of the compact to insure an advancing contact angle . . . . .	22
10. a. Phase diagram for the nickel-chromium <sup>29</sup> . . . . .	23
b. Phase diagram for the nickel-titanium system <sup>29</sup> . . . . .	23
11. Dimensions measured on photographic negatives of sessile drops. Two types are shown: for angles greater than 90° on the left, or less than 90° on the right . . . . .	25
12. Sessile-drop photographs of: (1) Pure Sherritt #C525 Ni, (2) Ni+0.3% Ti, (3) Ni+1.6% Ti, and (4) Ni+9.3% Ti. The magnification, 10x, has been reduced approximately 25 percent for reproduction. . . . .	28

FIGURES (cont'd.)

<u>No.</u>	<u>Page</u>
13. Sessile-drop photographs of: (1) Pure Sherritt #C525 Ni, (2) Ni+7% Cr, (3) Ni+10% Cr, and (4) Ni+19% Cr. The magnification, 10x, has been reduced approximately 25 percent for reproduction .	28
14. Graph of interfacial energy versus percent titanium . .	30
15. Graph of interfacial energy versus percent chromium . .	31
16. X-ray fluorescence curves. . . . .	34
17. X-ray powder pattern No. 1458 of interfacial material in Ni.-Ti experiments . . . . .	51
18. A.S.T.M. Card No. 2-1359 for $\alpha$ -Ti <sub>2</sub> O <sub>3</sub> . . . . .	52
19. X-ray powder patterns, Nos. 1489, 1485 and 1493. (Top - Pure Al <sub>2</sub> O <sub>3</sub> , Middle - Al <sub>2</sub> O <sub>3</sub> and unknown, Bottom - Solid solution of Cr <sub>2</sub> O <sub>3</sub> in Al <sub>2</sub> O <sub>3</sub> ) . . .	55
20. A.S.T.M. Card No. 5-0712 for $\alpha$ -Al <sub>2</sub> O <sub>3</sub> . . . . .	56
21. A.S.T.M. Card No. 6-0504 for Cr <sub>2</sub> O <sub>3</sub> . . . . .	57

TABLES

<u>No.</u>		<u>Page</u>
I.	Analyses of Materials . . . . .	15
II.	(a) Ni-Ti and Ni-Zr (Sherritt No. C 525 Ni used throughout) . . . . .	29
	(b) Ni-Cr Alloys (Sherritt No. C 525 Ni used throughout) . . . . .	29
III.	Wettability Data from Modified Procedures . . . . .	33
IV.	X-ray Fluorescence Analysis . . . . .	35
V.	Drying Agents and Drying Powers . . . . .	47
VI.	Data from Film No. 1458 . . . . .	52
VII.	Extinction Rules <sup>36</sup> for Space Group $D_{3d}^6 R3c$ . . . . .	53
VIII.	Calculated and Observed Data for Film No. 1458 . . . . .	54
IX.	Data from Film No. 1485 . . . . .	56

# AN INVESTIGATION OF BOND FORMATION BETWEEN ALUMINA SINGLE CRYSTALS AND NICKEL ALLOYS

## I. INTRODUCTION

### A. General Purpose and Scope

During the past decade, the development of metal-ceramic systems has been focused on the bonding of metals to refractory materials such as borides, carbides, nitrides, oxides, silicates, silicides, and ceramic mixtures. The important properties of many ceramic materials include corrosion and oxidation resistance, high melting points, and relatively high strength and creep resistance at elevated temperatures. Compared to metals, however, they are very brittle and sensitive to thermal shock. The ultimate aim of investigations in the metal-ceramic field is to produce combinations of metals and ceramics which are superior to either the metal or ceramic alone. At present, ceramic materials are commonly used in conjunction with metals as protective coatings on metal parts, as the refractory components of sintered powder mixtures known as "cermets", and as the finely dispersed phases of dispersion-hardened metals. The selection of promising materials appears to be based on bonding characteristics between the ceramic and metal phases. Although the properties of the metal-ceramic combinations have been measured, there is little fundamental basis for the selection of the components.<sup>1</sup> Hence, a study of the nature of the metal-to-ceramic bonds is necessary.

The fundamental factors<sup>2</sup> to be considered in an investigation of the mechanisms of bonding between metals and ceramics are: (1) chemical factors including wetting phenomenon and chemical reactions, (2) mechanical factors related to thermal expansion and bulk strengths, and (3) design factors involving size, shape and use of the final product. In this paper, the author considers chemical factors under two main headings, surface interactions and interfacial reactions.<sup>3</sup> Surface interactions are those associated with surface tension and wetting, and interfacial reactions are those related to the formation of interfacial solid solutions and chemical compounds.

Physical wetting of the ceramic by the metal is a major factor in producing an effective bond. Wetting can be studied by considering the interfacial energy involved. In general, a low interfacial energy is associated with a strong metal-ceramic bond. It should be noted, however, that other factors such as interfacial stresses arising from heating or cooling often render a strong bond ineffective.

Because lower interfacial tensions increase the probability of forming an effective bond, a method of detecting changes in this quantity is essential. The sessile-drop method<sup>4,5,6,7</sup> can be employed very effectively for measurements of this type at high temperatures. The forces acting at the interface of a sessile drop of liquid metal on a smooth ceramic surface are related according to the equation:<sup>8</sup>

$$\gamma_{SL} = \gamma_{SV} - \gamma_{LV} \cos \theta \quad (1)$$

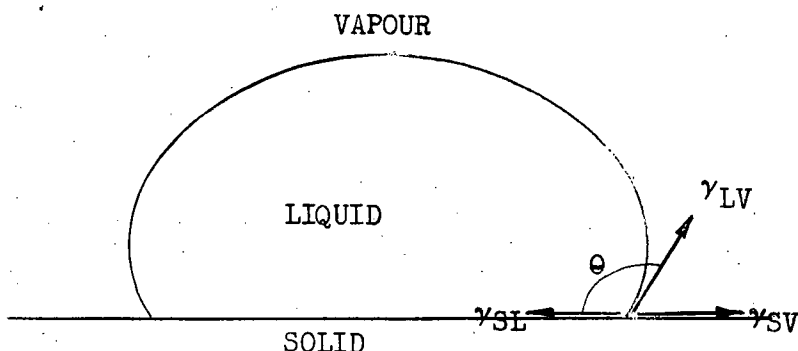


Figure 1. Surface tension forces acting on a sessile drop.

where  $\gamma_{SL}$  is the interfacial energy,  $\gamma_{SV}$  is the surface energy of the ceramic,  $\gamma_{LV}$  is the surface energy of the liquid metal and  $\theta$  is the angle of contact or wetting angle (see Figure 1). For many of the metals and ceramics of interest for practical uses, very little data is available on the individual surface energies. This has limited the choice of systems for the measurement of variations in interfacial energy. The measure of the attraction between two different materials is the work of adhesion. This can be calculated directly from experimental data by the following equation:

$$W_{ad} = (\gamma_{LV} + \gamma_{SV}) - \gamma_{LS} = \gamma_{LV}(1 + \cos \theta) \quad (2)$$

where  $W_{ad}$  is the work of adhesion. Thus, the surface tension of the metal is of major importance. Available surface tension values indicate that surface tensions of liquid metals are approximately twice those of the solid oxides.<sup>3</sup>

The important interfacial reactions are the formation of solid solutions and the production of definite chemical compounds at or near the metal-ceramic interface. These reactions are often essential to the formation of an effective bond in conjunction with surface interactions.<sup>9</sup> Modifications of the material present at the interface change the bonding forces. The chemical reactions which modify the interface depend on the thermodynamics of the system.<sup>10,11</sup> Unfortunately, thermodynamic data is usually incomplete or non-existent for the systems and elevated temperatures of interest. A study of interfacial compounds must often be accomplished by experimental methods only. Similarly, solid solutions formed from the metal phase at the interface usually cannot be definitely predicted from thermodynamic data alone.<sup>3</sup>

The choice of the metal-ceramic systems for the investigation of bond mechanisms is, therefore, limited primarily by lack of thermodynamic data at elevated temperatures for both the ceramic and metal components. Recently, however, thermodynamic investigations have been completed on the aluminum oxide-nickel alloy systems.<sup>7,12,13,14</sup> Consequently, these materials were chosen for an investigation into the mechanisms of bond formation.

#### B. Previous Investigations.

Prior work indicates that alloys of nickel, chromium, titanium and zirconium bond to aluminum oxide. In many cases, the aluminum oxide was used in the powdered or sintered form

without regard for some important experimental variables. Many investigators were concerned only with production of a strong bond for engineering applications and not with the mechanisms of bond formation. Only the fundamental work will be cited here.

The sessile-drop technique was used extensively by Kingery and co-workers 7,12,13,15,16 in a thorough study of surface interactions between sintered alumina and various metals and alloys. Surface energies and interfacial energies were measured in the systems. Measurements indicated that the more electropositive components of alloys, which were selectively adsorbed at the liquid metal-solid ceramic interface, decreased the interfacial energy. In a narrow concentration range, the selective adsorption caused a marked decrease in the interfacial energy. The critical concentrations were believed to be approximately equivalent to the activities at which a monolayer of the more electropositive atoms was present at the interface.

The excess interfacial concentration can be calculated from Gibbs' equation at constant temperature and pressure,<sup>8</sup>

$$-d\gamma = \Gamma_1 du_1 + \Gamma_2 du_2 \quad (3)$$

where  $\Gamma_1$  and  $\Gamma_2$  are the excess interfacial concentrations of the two components,  $u_1$  and  $u_2$  are the chemical potentials of the components of the system, and  $\gamma$  is the surface tension. For dilute solutions, the chemical potential of the major component,  $u_1$ , is constant and the chemical potential of the solute,  $u_2$ , is given by,

$$\mu_2 = \text{constant} + R T \ln c_2 \quad (4)$$

The change in the chemical potential of the solvent,  $\mu_1$ , is approximately zero. Thus, combining equation (3) and (4) results equation:

$$-d\gamma = \Gamma_2 RT d \ln C_2 \quad (5)$$

where R is the gas constant, T is the absolute temperature and  $C_2$  is the concentration of the solute. This equation can be applied to nickel-chromium,<sup>13</sup> and nickel-titanium<sup>12,13</sup> alloys melted on alumina supports.

Figure 2 illustrates some of results to which the above theory has been applied. Most Ni-Ti experiments were done by Allen and Kingery,<sup>12</sup> and the Ni-Cr experiments were done by Kurkjian and Kingery.<sup>13</sup> Measurements were made at 1475°C. using sintered alumina as the ceramic supports. The surface energy of solid alumina used for calculation of interfacial energies was known to a good approximation<sup>17</sup> to be 905 ergs per cm.<sup>2</sup> at 1850°C. (assuming a temperature coefficient of -0.1 ergs per cm.<sup>2</sup> per °C). The surface energy calculated for pure nickel in a vacuum was 1725 ergs per cm.<sup>2</sup> at 1475°C. This compares favourably with other recent values.<sup>7,18</sup> Since the surface energies of titanium and chromium are similar to the surface energy of nickel, small additions of titanium and chromium to nickel do not appreciably affect the surface energy of the nickel. The temperature coefficients of surface energies of liquid metals are, in general, very small<sup>19</sup> and the temperature coefficients of interfacial energies for nickel and nickel alloys are about -1.0 ergs per cm.<sup>2</sup> per °C.<sup>12</sup>

Reactions between the metals and oxides were

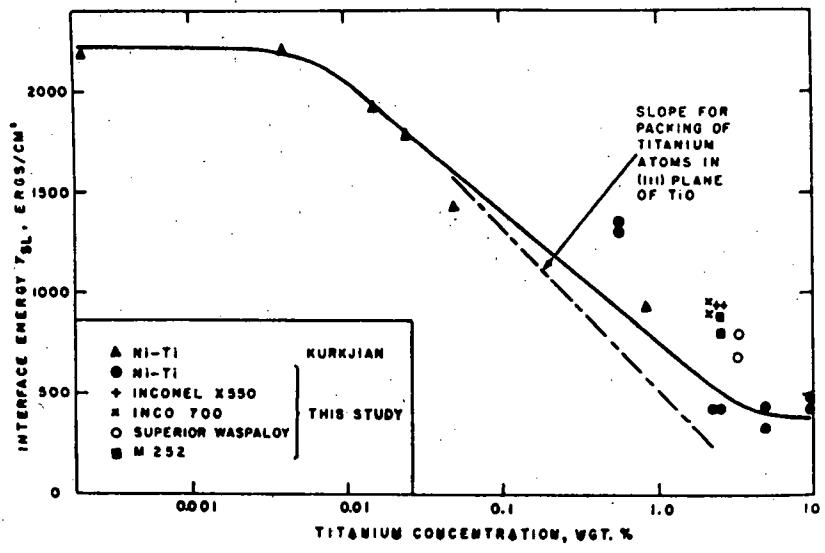
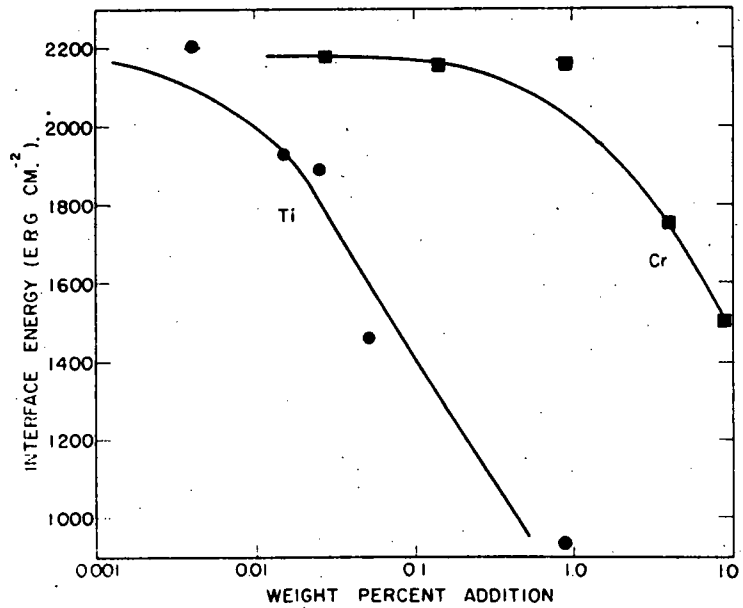


Figure 2. Graphs reproduced from the work by Allen and Kingery, and Kurkjian and Kingery.

thoroughly investigated by Economos and Kingery.<sup>9</sup> Sintered ceramics were used in their investigation as closed reaction chambers under vacuum. Metals were heated to temperatures greater than 1400°C and the resulting reaction products were microscopically observed. Although nickel forms a  $\text{NiO} \cdot \text{Al}_2\text{O}_3$  spinel when heated in contact with alumina in an oxidizing atmosphere,<sup>20</sup> Economos and Kingery found no reaction at the nickel-alumina interface under a vacuum. Zirconium showed considerable corrosion of the oxide, penetration along grain boundaries and black discoloration of the grains at 1800°C but no new phase was formed at the interface. Similar results were obtained with titanium at 1800°C but no appreciable attack of the alumina by titanium was noticed below 1600°C. According to calculations, titanium should react extensively with all oxides except  $\text{ThO}_2$  and  $\text{BeO}$ .

Baxter and Roberts<sup>14</sup> do report an interface alteration when nickel-titanium alloys were heated to 1490°C in contact with sintered alumina. The alumina surface was colored from brown to blue-black which was presumably due to the formation of  $\text{TiO}_{1.25}$  - light brown,  $\text{TiO}_{1.44-1.33}$  - dark brown, and  $\text{TiO}_{1.73-1.65}$  - blue-black. But, the formation of these lower oxides of titanium adversely affected the bond strength.

Considerable attention has been given to the alumina-chromium system. Changes in the composition of the oxide phase result in the formation of a  $\text{Cr}_2\text{O}_3$ - $\text{Al}_2\text{O}_3$  solid solution.<sup>2,3</sup> This combination of a few percent by weight of  $\text{Cr}_2\text{O}_3$  in the  $\text{Al}_2\text{O}_3$  (see Figure 3) surface appears to be an essential step in the

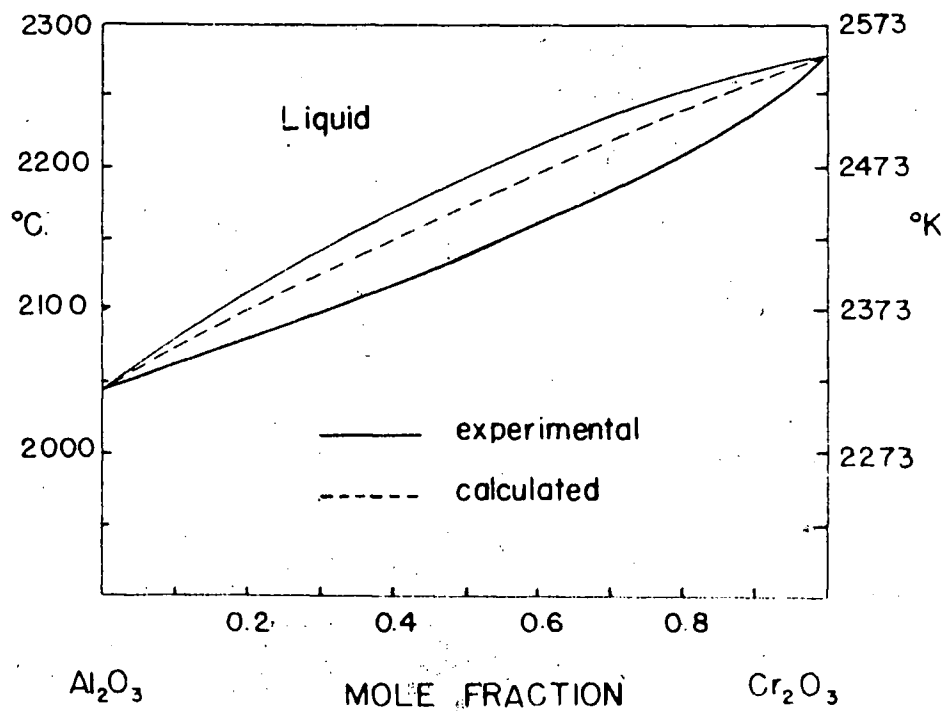


Figure 3. A phase diagram for the  $\text{Cr}_2\text{O}_3$ - $\text{Al}_2\text{O}_3$  system.<sup>21</sup>

formation of a strong bond. The free energy change on formation of the solid solution is of the correct order of magnitude to reduce the interfacial energy the required amount to promote wetting. Microscopic examination of the interface shows no evidence of intermediate phases or diffuse boundary regions. In effect, the chromium is bonded to the  $\text{Cr}_2\text{O}_3$ - $\text{Al}_2\text{O}_3$  solid solution rather than the  $\text{Al}_2\text{O}_3$  ceramic. However, there is no fundamental reason why chromium should have a greater affinity for the  $\text{Cr}_2\text{O}_3$ - $\text{Al}_2\text{O}_3$  solid solution than for  $\text{Al}_2\text{O}_3$ .

A somewhat different approach to the study of the nature of the bond has been taken by Pincus.<sup>22</sup> He studied the metal-ceramic interactions between molybdenum and aluminum oxide

with the aid of taper sections and X-ray patterns. The reactions of Mo and MoO<sub>3</sub> with pure alumina single crystals and sintered mixtures were investigated. X-ray diffraction powder patterns indicated that a new phase, Al<sub>2</sub>(MoO<sub>4</sub>)<sub>3</sub>, was formed by an interfacial reaction if a controlled degree of metal oxidation was allowed.

It can be seen from the above survey that, although various methods have been used to study the nature of metal alumina bonds, little can be said about them that is fundamental or conclusive. Similarly, general rules which would apply to all metal-ceramic systems have not been developed. Each system must, therefore, be studied separately in order to evaluate the mechanism involved in bonding.

### C. Specific Aims of the Present Investigation

The original purpose of this investigation was to study bond formation between single crystals of Al<sub>2</sub>O<sub>3</sub> (sapphire) and, various metals and alloys. A consideration of substitutional diffusion of the metal ion into the aluminum oxide lattice and of reduction of the aluminum oxide by reactive metals was to be of prime importance. Likely elements for substitutional diffusion would be those which have: (1) favorable sizes for diffusion, (2) similar M<sub>2</sub>O<sub>3</sub> oxides, and (3) oxides which are stable above the melting point of the metal. Elements which meet all three conditions are: manganese, iron, chromium, vanadium, molybdenum, gallium, titanium and bismuth. The reactive metals commonly used to promote bonding are: titanium, zirconium, tantalum and columbium.

All of the above possibilities were to be investigated by measurements of contact angle of a sessile drop of liquid metal on the sapphire. The examinations of the bond were to be made by metallographic, crystallographic and tracer techniques. However, preliminary experiments indicated the possibility of numerous experimental difficulties. The field of investigation was, therefore, narrowed in order to allow a detailed study of the systems used.

Titanium and chromium of the first group of elements mentioned previously, and, zirconium and titanium of the second group were chosen for the study surface interactions and interfacial reactions. It was hoped that the use of single-crystal, sapphire plaques of controlled crystallographic orientation would lead to a more fundamental understanding of the effect of interfacial energy on bond formation. For the same reason, the Debye-Scherrer X-ray diffraction analyses and X-ray fluorescence analyses were planned for identification of reaction products at the metal-ceramic interface. With this approach, the chemical factors influencing the bond formation should be detected.

## II. EXPERIMENTAL

### A. Materials

#### 1. Aluminum Oxide

The single crystal plaques of aluminum oxide used throughout the investigation were high purity synthetic sapphire (99.99%  $\text{Al}_2\text{O}_3$ ) supplied by Linde Air Products Co., Ltd. This material is available in the form of windows, rods, tubing and special shapes. The rods used in this work were of controlled orientation specified within  $\pm 5$  degrees.<sup>23</sup>

The crystal structure of sapphire is based on a hexagonal closest packing of atoms.<sup>24</sup> The oxide ions are very nearly in a hexagonal closest packing with the aluminum ions in the octahedral interstices of the oxygen framework. Because the number of aluminum ions is different than the number of oxygen, one-third of the octahedral sites are vacant. The arrangement of filled and empty interstices, however, is ordered (see Figure 4). Small amounts of impurity elements in the octahedral interstices produce characteristic colors. A sapphire-blue color is produced by 0.001 to 0.1% titanium,<sup>25</sup> a ruby red by less than 8 mole percent of  $\text{Cr}_2\text{O}_3$  in solid solution with  $\text{Al}_2\text{O}_3$ , and a light green by more than 8 mole percent  $\text{Cr}_2\text{O}_3$ .<sup>26</sup>

For the experiments, sapphire rods, 0.35 inches in diameter, were used to make the ceramic supporting plaques. These rods were supplied with the rod axis at  $60 \pm 5$  degrees to the crystallographic c-axis. Cutting the rods perpendicular to the rod axis produced a working surface approximately coincident to

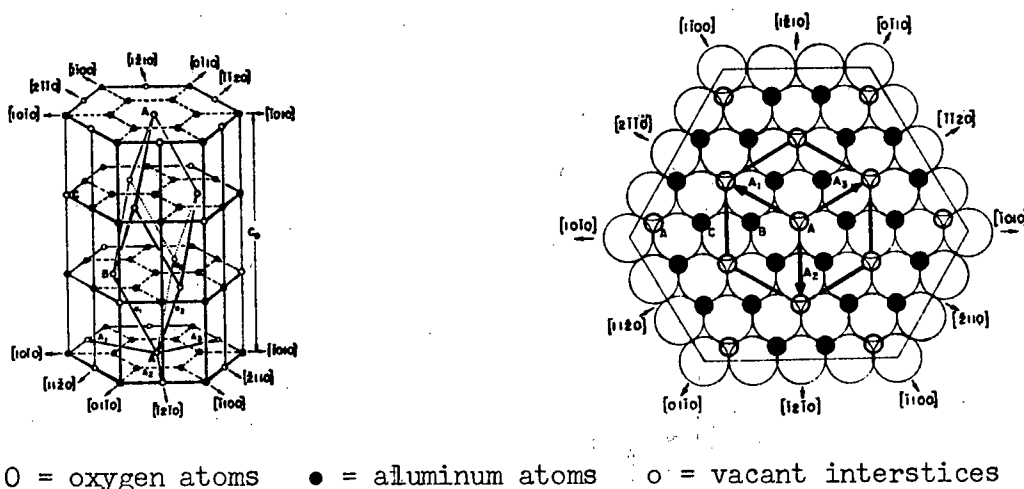


Figure 4. Pictorial representation of sapphire lattice.<sup>24</sup>

the  $\langle 10\bar{1}2 \rangle$  plane. The direction perpendicular to this plane is the preferred growth direction. The basal plane is the closest packed plane for sapphire.

## 2. Metals.

All the metals used in this work were obtained in the powder form. Nickel, the major constituent in the alloys used, was supplied by Sherritt Gordon Mines Ltd, and Mond Nickel Co., Ltd. Chromium powder coated with nickel was also supplied by Sherritt Gordon Mines Ltd. The titanium hydride and zirconium hydride powders used to make nickel-titanium and nickel-zirconium alloys were obtained from Metal Hydrides Incorporated. The chemical analyses of these materials are given in Table I.

TABLE I

Analyses of Materials

Material	Analysis (Maximum percent)															
	Ni	Ti	Cr	Zr	Co	Cu	Fe	S	C	H <sub>2</sub>	N <sub>2</sub>	Ca	Mg	Al	Si	Other
Titanium hydride		95		0.1						3.5	0.2	0.05	0.05	0.1	0.1	
Zirconium hydride		0.1		95.5			0.15	0.01	0.15	2.1	0.7	0.05	0.03	0.15	0.03	
Nickel coated chromium	79.6		19.0		0.57		0.003	0.018	0.01							
Sherritt Ni #C 525	Bal.				0.08	0.029	0.022	0.016	0.01							<.005
Sherritt high purity Ni	Bal.				0.008	0.009	.004	0.006	.08							
Mond carbonyl Ni	Bal.				0.005	0.008	0.007	0.002	0.091							<.003

B. Apparatus

The apparatus was designed with the following objectives: (1) to produce temperatures as high as 1800°C by induction heating and vacuums as high as  $5 \times 10^{-5}$  m.m. of Hg, (2) to permit the introduction of reducing atmospheres at pressures less than atmospheric pressure, and (3) to allow accurate measurements on sessile drops at temperatures greater than the melting points of the alloys used. The equipment is shown in Figures 5 and 6.



Figure 5. The apparatus assembly of the induction furnace, vacuum system and optical system.

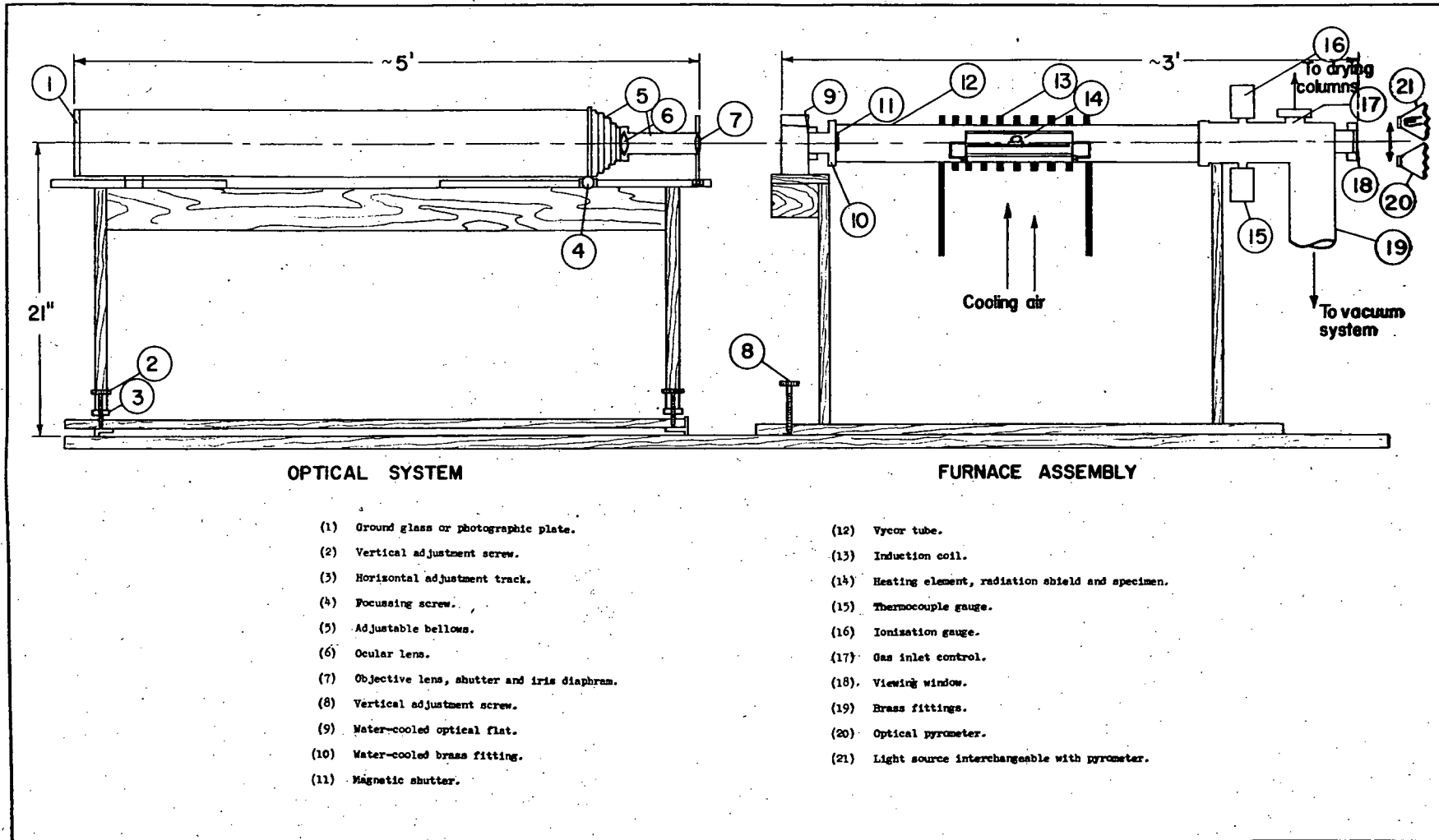


Figure 6. Assembly drawing of the apparatus.

## 2. Furnace.

The heating elements of the furnace were constructed from 0.005 inch molybdenum sheet (see Figure 7). The susceptor



Figure 7. Molybdenum heating elements (dismantled) of the induction furnace.

consisted of a "closed loop" in the form of a cylinder 0.75 inches in diameter and 3.5 inches long, open at both ends. A radiation shield surrounded the susceptor to prevent excessive heat loss from the core of the heating element. This shield consisted of an "open loop" cylinder 1.5 inches in diameter and 5 inches long, also open at both ends. The susceptor and radiation shield assembly was supported inside the induction coil by a molybdenum-rod framework. This rod was separated from the vycor tubing containing the heating elements by sintered alumina insulators.

The furnace-tube assembly consisted of a vycor (fused silica) tube,  $2\frac{1}{2}$  inches in diameter and 18 inches in length. Rubber O-ring seals and silicone high vacuum grease were used in the vycor-to-brass joints at the end of the tube.

At the camera end of the furnace, a water-cooled optical flat was used to protect the camera lenses from heat radiation. Because of the high vapour pressures of metals at operating temperatures,<sup>27</sup> a magnetic shutter was placed inside the furnace to protect the optical flat from metal vapours. At the other end of the furnace, a viewing window was built into the elbow leading to the vacuum system. Outside this window, a light source and an optical pyrometer were placed such that either could be positioned on the centre-line of the furnace.

Through a water-cooled, copper induction coil ( $\frac{1}{4}$  inch O.D. tubing, 21 turns) around the outside of the vycor tube, power was supplied to the heating element by a high-frequency induction generator. This unit, Lepel model T-10-3, produces power from 0 to 23.5 K.V.A. at 400,000 cycles per second. The power could be adjusted precisely by varying either the plate current or the grid current in the tube of the generator. The resulting temperature in the furnace was measured to  $\pm 5^{\circ}\text{C}$  by a Hartmann and Braun pyrometer, model TO-10-e. Emissivity corrections were not necessary because of the design of the susceptor. Power input to the furnace was limited by the loss of strength of the vycor tube at elevated temperatures. The tube was, therefore, air-cooled by means of a 10 inch diameter fan.

## 2. Vacuum system.

The pumping system was designed to produce a high vacuum or a controlled low vacuum. A mechanical fore pump and a two-stage oil diffusion pump produced vacuums in the range of  $10^{-4}$  to  $10^{-5}$  m.m. Hg. With only the fore pump operating, a reducing

atmosphere could be continuously flushed through the system to maintain a vacuum of 0.5 m.m. of Hg. The high vacuums were measured with an N.R.C. ionization gauge, type 507, and the low vacuums were measured by an N.R.C. thermocouple gauge, type 501.

Purified reducing atmospheres were obtained by continuously flushing dry hydrogen through the system. The hydrogen was supplied by Canada Liquid Air Co., Ltd. in 2000 p.s.i. tanks. The gas was purified at a controlled rate of less than one cubic foot per minute. The purification and drying train consisted of a hydrogen "deoxo" cartridge in series with columns of anhydrous calcium sulphate, silica gel, and phosphorous pentoxide. The "deoxo" cartridge converted the oxygen impurity to water. The silica gel and anhydrous calcium sulphate reduced the water concentration in the hydrogen to 0.005 milligrams per liter of gas and the phosphorous pentoxide reduced the concentration further to less than 0.0002 milligrams per liter. (See Appendix I)

### 3. Optical system.

At temperatures of greater than  $1100^{\circ}\text{C}$ , objects emit enough light to produce an outline image on a photographic film. Sharp images of the incandescent sessile drops in this investigation could be readily obtained at  $1500^{\circ}\text{C}$  if a camera were correctly designed for this purpose.

A camera was constructed to give a ten-fold magnification. This was accomplished by the combination of a two-component, objective lens (focal length of 11 inches) and a single component, ocular lens (focal length of 42 millimeters). The fixed,

objective lens was equipped with an adjustable shutter and iris diaphragm. The ocular lens was separated from the objective lens by a 10 to 15 inch adjustable bellows, and from the ground glass plate by a 42 to 48 inch adjustable bellows. The camera was positioned so that the optical axis was in the plane of the ceramic surface and parallel to axis of the furnace by means of vertical adjustment screws and horizontal adjustment tracks. These were securely fixed to the camera frame. Because of the length of the camera, sensitivity to vibrations was high and a very sturdy framework was necessary.

Focusing adjustments were made by means of a screw-thread adjustment on the ocular lens holder which moved parallel to the optical axis of the camera. Before the specimen was heated, preliminary focusing was accomplished with the aid of a light source at the far end of the furnace. The light source produced a silhouette of the specimen on the ground glass.

### C. Preparation of Materials.

The single-crystal aluminum oxide was obtained as sapphire rods. Discs, approximately  $1/8$  inch thick, were cut from the rod perpendicular to rod axis with a Felker "Di-Met" diamond saw. These discs were mounted in lucite and were polished with diamond powder suspended in kerosene. Rough polishing was done with 325-micron diamond powder in kerosene on plate glass (see Figure 8a).

Fine polishing was completed with the aid of a vibratory polisher.<sup>28</sup> The bottom of the polishing bowl was covered with a

heavily-etched copper plate. A mixture of diamond paste ( $\frac{1}{4}$  micron) and kerosene was used as the polishing compound. After 48 to 72

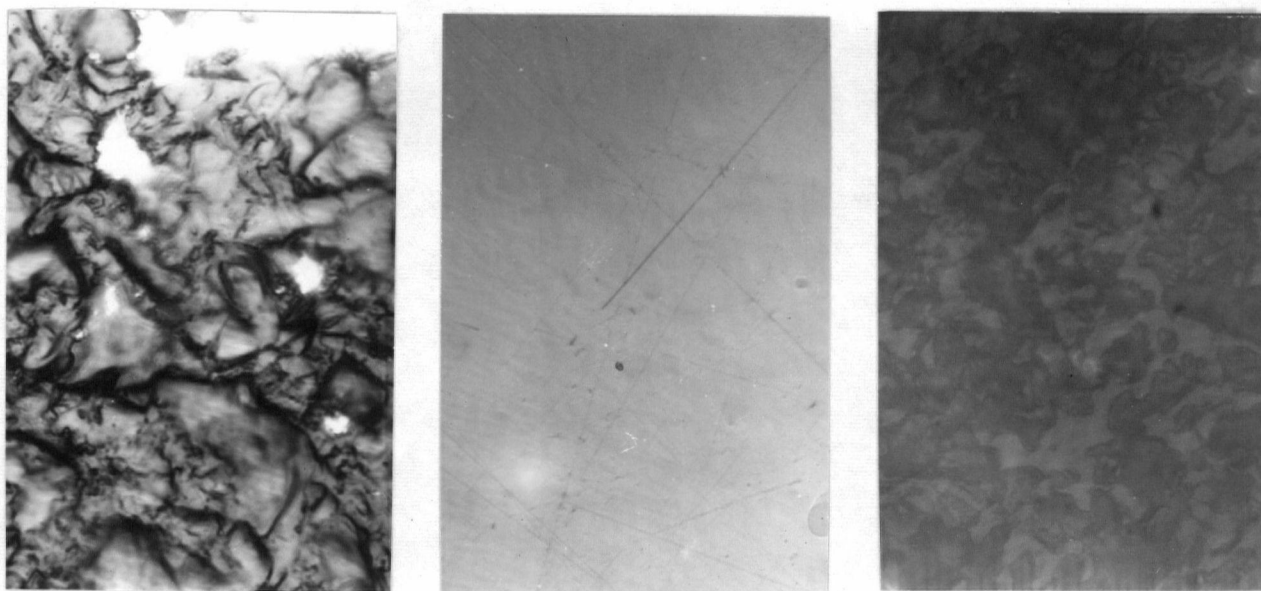


Figure 8. (a) Rough-polished surface of sapphire rod  
(b) Finished surface of sapphire rod  
(c) Finished surface of sintered aluminum oxide. Magnification 1000x

hours of continuous polishing, a suitable surface was obtained (see Figure 8b). The discs were then broken away from the lucite mounting.

The polished plaques were soaked in concentrated nitric acid and washed with ethyl alcohol and acetone. Care was taken in handling the plaques to avoid contamination of the polished surface. Metal tweezers were used whenever possible. The same precautions were necessary in the handling of the metals because minute amounts of contaminants often affect surface energy measurements greatly.

Metal powders, mixed in the desired proportions, were

compacted in a cylindrical die,  $\frac{1}{4}$  inch in diameter, under a pressure of 40 tons per square inch. The compacting die was machined to form a compact of a shape required to insure an advancing contact angle when the alloy melted (see Figure 9). The die cavity was designed to hold 0.5 to 0.7 grams of powder. Clean metal tools were used throughout to avoid contamination of the compact.

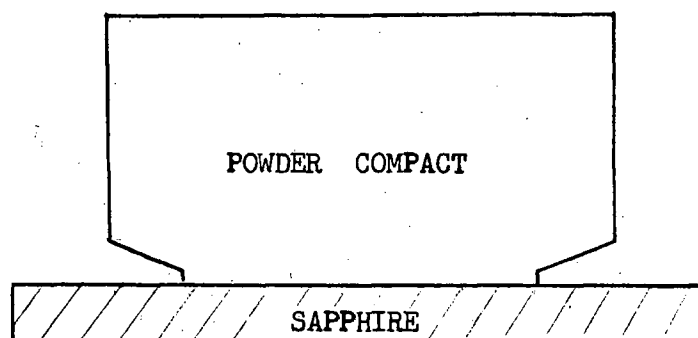


Figure 9. Cross-sectional view of a specimen showing shape of the compact to insure an advancing contact angle.

For contact angle measurements on the nickel-titanium and nickel-chromium alloys, compositions were used within the solid-solubility limits. The solid-solubility ranges are 0 to 10.8 percent titanium in the nickel-titanium system (see Figure 10a) and 0 to 47 percent chromium in the nickel-chromium system (see Figure 10b). The compositions of nickel-zirconium, which were investigated, were similar to those of nickel-titanium.

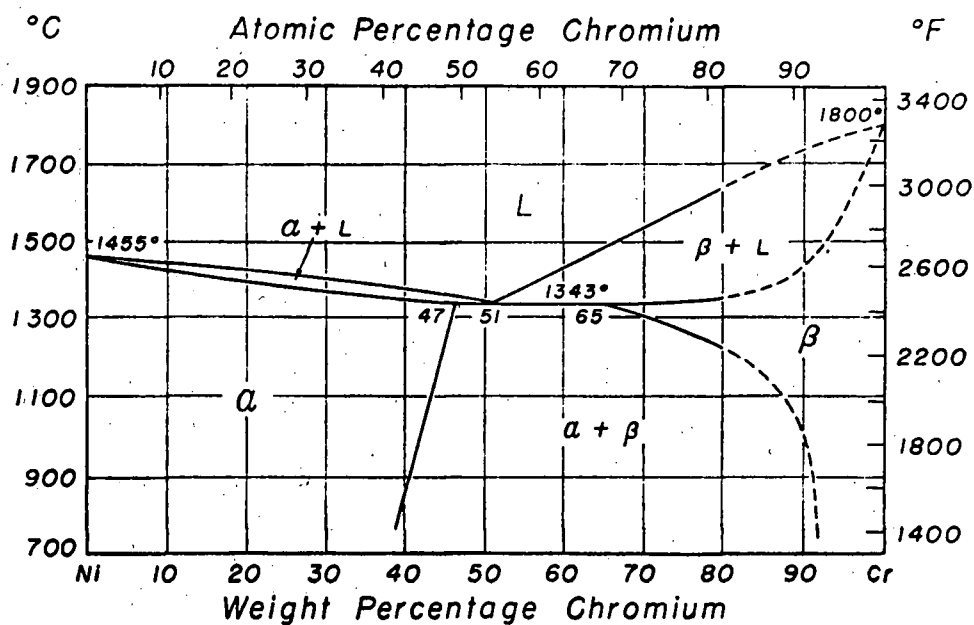


Figure 10b. Phase diagram for the nickel-chromium system.<sup>29</sup>

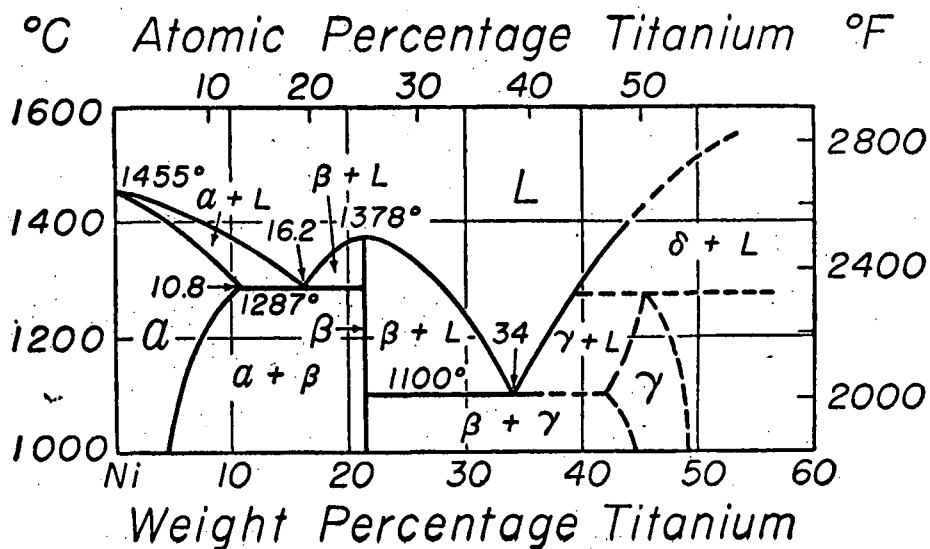


Figure 10a. Phase diagram for the nickel-titanium system.<sup>29</sup>

#### D. Experimental Procedure.

##### 1. Sessile-drop experiments.

The metal was placed on the polished sapphire inside the susceptor. With the aid of the light source, the specimen was leveled. The furnace was assembled and pumped to a fore pump vacuum of  $5 \times 10^{-3}$  m.m. of Hg. Purified hydrogen was then flushed through the furnace at a rate sufficient to maintain a vacuum of 0.5 mm. of Hg. The temperature was slowly raised to approximately  $800^{\circ}\text{C}$ . Near this temperature, the hydrogen gas ionized and hydrogen-ion cleaning of the specimen took place. After a heating period of 10 minutes, the power was turned off and the system was pumped down to a vacuum of  $10^{-5}$  m.m. Hg. The power was again slowly increased until the temperature reached  $1500^{\circ}\text{C}$  as measured by the optical pyrometer. The specimen was maintained at this temperature for 20 minutes to insure equilibrium conditions.<sup>16,30</sup> During the holding time, the image of the sessile drop was carefully focused on the ground glass. At the end of the heating period, the ground glass was replaced by a Kodak "M" plate, the fore pump and fan were turned off to reduce vibrations, and the photographic plate was exposed. The power was then decreased to zero and the furnace was allowed to cool slowly to room temperature.

The sessile-drop method of calculating surface tensions and contact angles involves the measurement of the dimensions of a stationary liquid drop on a smooth flat surface. From the measurements indicated in Figure 11, sufficiently accurate calculations<sup>31</sup> can be made by a method described later.

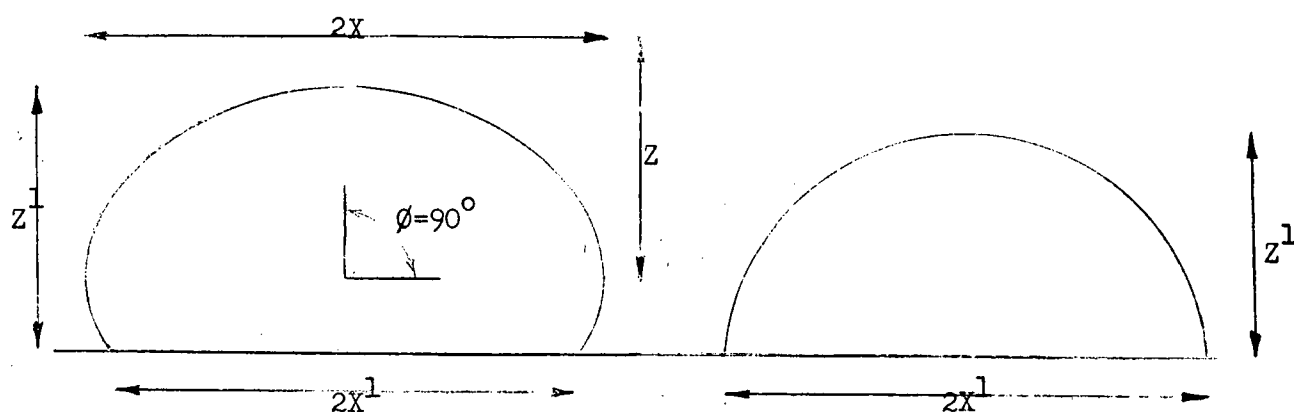


Figure 11. Dimensions measured on photographic negatives of sessile drops. Two types are shown: for angles greater than  $90^\circ$  on the left, or less than  $90^\circ$  on the right.

For measurements on the photographic plates, the plates were mounted on the illuminated window of a standard viewing box. Measurements were made with dividers and microcalipers to the nearest 0.001 inch.

## 2. X-ray fluorescence examinations.

In the nickel-titanium and nickel-chromium experiments, some specimens were selected for examination by X-ray methods. After separation of the metal and sapphire, X-ray fluorescence analyses were made on the mating surfaces of the metal drop and the sapphire plaque. The interfacial surfaces were analyzed for nickel, titanium, and chromium to investigate selective adsorption at the interface. A tungsten-target X-ray tube (40 K.V., 20 m.a.) and a lithium fluoride analyzing crystal were used. The results were recorded in graphical form by a scintillation counter.

## 3. X-ray diffraction investigations.

Following the X-ray fluorescence analyses, the inter-

facial layers on the sapphire were cleaned and prepared for identification by the X-ray powder method. The powder patterns were obtained by exposures to copper radiation (40 K.V., 15 m.a.) for 2 to 4 hours. These patterns were indexed and compared with patterns of standard materials recorded in the A.S.T.M. card index for powder patterns.

### III. EXPERIMENTAL RESULTS AND CALCULATIONS

#### A. Wetting Results.

To calculate interfacial energy data, precise measurements of surface energies and contact angles are required. The sessile-drop dimensions,  $X$ ,  $Z$ ,  $X^1$ , and  $Z^1$  (see Figure 11), were used to calculate contact angles and surface energies by the methods outlined in Appendix II. The variations of contact angle for the nickel-titanium and nickel-chromium systems are illustrated in Figures 12 and 13 and listed in Table II. The average liquid surface energy value for these alloys was 1845 ergs per cm.<sup>2</sup> calculated from drop dimensions. By substituting the appropriate values of contact angle and the values of surface energy,  $\gamma_{LV} = 1845$  ergs per cm.<sup>2</sup> and  $\gamma_{SV} = 940$  ergs per cm.<sup>2</sup>,<sup>17</sup> into equation (1), the respective interfacial energies can be calculated. These interfacial energies have been listed in Table II and plotted in Figures 14 and 15.

Although a number of nickel-chromium alloys were used, none of the experiments involving zirconium were entirely successful. The alloys either erupted after melting or reacted violently with the sapphire to form a rough scale on the metal drop. Precise measurements on the resulting photographs were inaccurate or impossible. Therefore, only one contact angle was measured (see Table IIa) and no interfacial energies were calculated.

Considerable differences between the above data and previous values for nickel-titanium and nickel-chromium alloys on

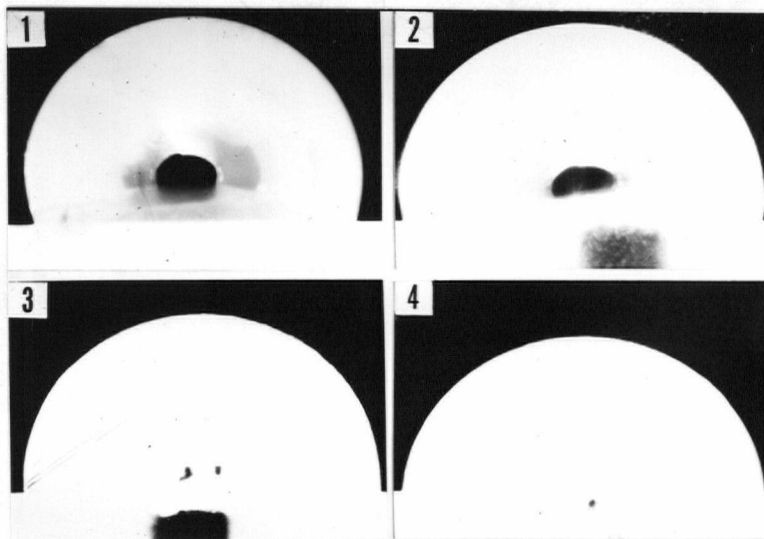


Figure 12. Sessile-drop photographs of: (1) Pure Sherritt #C525 Ni, (2) Ni + 0.3% Ti (3) Ni + 1.6% Ti, and (4) Ni + 9.3% Ti. The magnification, 10x, has been reduced approximately 25 percent for reproduction.

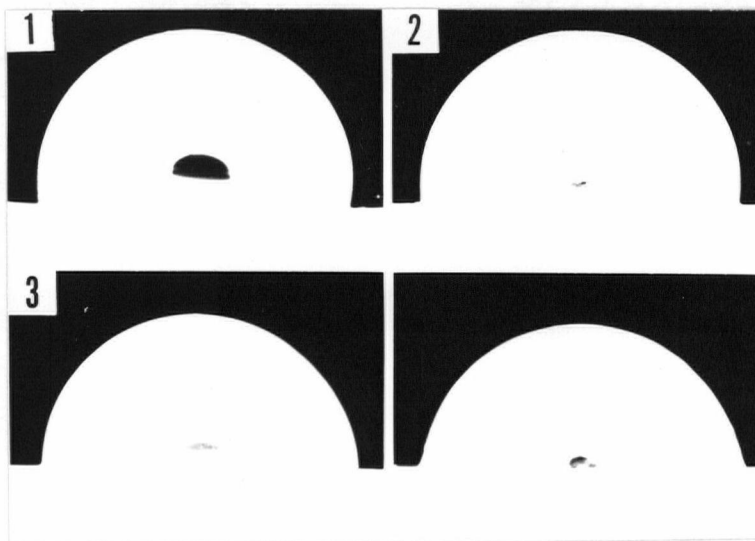


Figure 13. Sessile-drop photographs of: (1) Pure Sherritt #C525 Ni, (2) Ni + 7% Cr, (3) Ni + 10% Cr, and (4) Ni + 19% Cr. The magnification, 10x, has been reduced approximately 25 percent for reproduction.

TABLE II

Experimental Wettability Data.

(a) Ni-Ti and Ni-Zr (Sherritt No.C525 Ni used throughout)

Alloy	$\theta$ (deg.)	$\gamma_{SL}$ (ergs cm. <sup>2</sup> )
Pure Ni	108.0 (av.)	1510
Ni + 0.3% Ti	101.6	1311
Ni + 1.0	97.4	1178
Ni + 1.2	95.1	1104
Ni + 1.40	92.4	1017
Ni + 1.42	85.7	800
Ni + 1.44	105.7	1439
Ni + 1.6	90.0	940
Ni + 1.8	85.3	789
Ni + 1.9	87.6	863
Ni + 2.1	85.1	782
Ni + 3.4	90.0	940
Ni + 3.7	82.9	713
Ni + 4.1	89.9	938
Ni + 4.8	87.9	874
Ni + 7.1	87.5	860
Ni + 8.4	83.6	735
Ni + 8.5	85.6	798
Ni + 9.3	80.1	623
Ni + 10.4% Zr	75 (approx.)	

(b) Ni-Cr Alloys (Sherritt No.C525 Ni and Sherritt Ni coated Cr used).

Alloy	$\theta$ (deg.)	$\gamma_{SL}$ (ergs cm. <sup>2</sup> )
Pure Ni	108.0 (av.)	1510
Ni + 2% Cr	101.1	1295
Ni + 2	107.7	1501
Ni + 4	106.4	1461
Ni + 6	105.9	1446
Ni + 7	100.7	1283
Ni + 8	96.2	1139
Ni + 8	97.4	1178
Ni + 9	99.5	1117
Ni + 9	89.1	911
Ni + 10	86.7	834
Ni + 10	87.3	853
Ni + 11	88.3	885
Ni + 11	89.0	908
Ni + 12	84.9	776
Ni + 14	90.0	940
Ni + 14	82.3	725
Ni + 14	84.8	773
Ni + 19	82.3	725
Ni + 19	82.1	690
Ni + 19	84.1	750

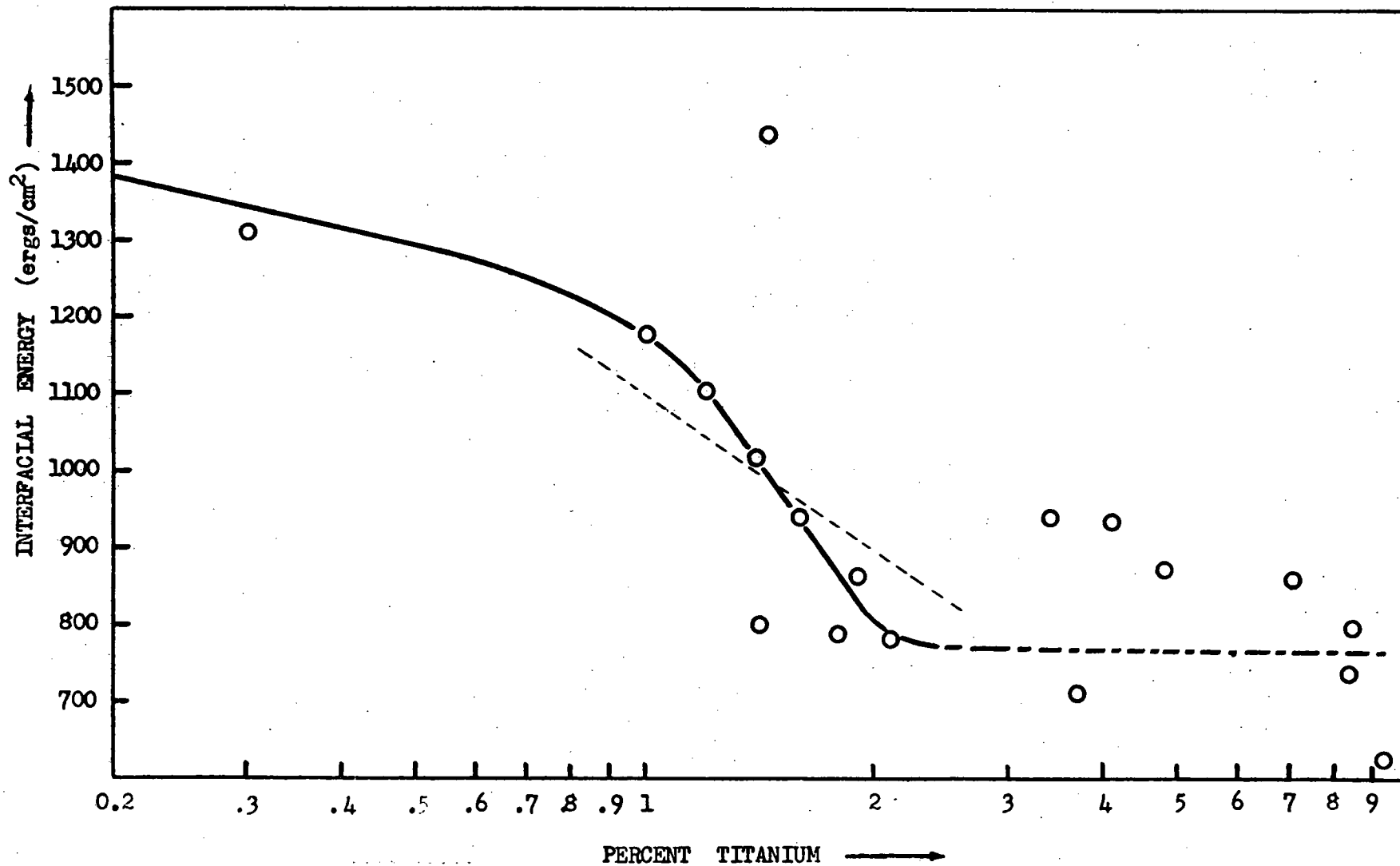


Figure 14. Graph of interfacial energy versus percent titanium.

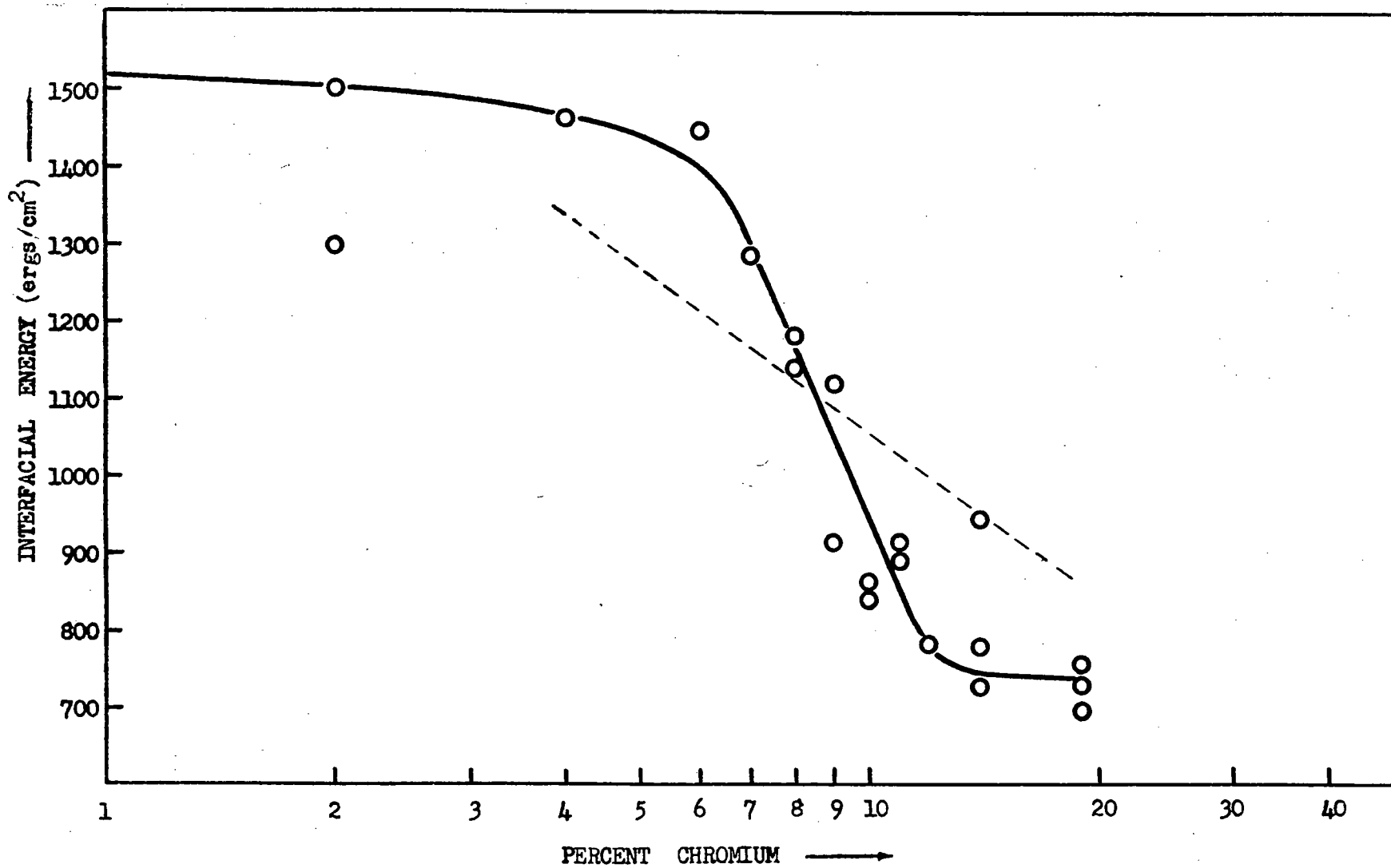


Figure 15. Graph of Interfacial Energy versus Percent Chromium

sintered alumina supports are apparent. The interfacial energies of the pure nickel and low-alloy samples appear to be too low<sup>12,13</sup> and the high-alloy interfacial energies appear too high.<sup>12</sup> Possible causes of these differences are: (1) surface condition of the ceramic support,<sup>8</sup> (2) size of the metal drop,<sup>31</sup> (3) orientation of the ceramic support, and (4) purity of the metals.<sup>15</sup> Experiments were, therefore, designed to investigate these possibilities. The modifications and the resulting changes have been listed in Table III. The three types of ceramic surfaces used for investigating surface and orientation effects are shown in Figure 8. Analyses for the different grades of nickel used for the modification of metal purity are listed in Table I.

The surface energy calculated for the Sherritt high-purity nickel is 1595 ergs per cm.<sup>2</sup> and the corresponding value for the Mond carbonyl nickel is 1725 ergs per cm.<sup>2</sup> The difference between these values and the value for Sherritt No. C525 nickel (1845 ergs per cm.<sup>2</sup>) is probably due to the different concentrations of surface-active impurities such as carbon and sulphur in the metal.

## B. X-ray Data.

### 1. X-ray fluorescence analyses.

Metal and ceramic specimens were selected for analyses from the Ni + 2.1% Ti and Ni + 10% Cr experiments. The resulting curves, which have been reproduced in Figure 16, show that titanium and chromium concentrations are higher at the ceramic surface than in the metal drop compared to the respective nickel

TABLE III

Wettability Data from Modified Procedures

Metal	Approximate metal weight	Ceramic support	$\theta$ (deg.)	$\gamma_{SL}$ ergs/cm <sup>2</sup>	Variable
#C525 Ni	0.5 gms.	Fine-polished sapphire disc	108.0	1510	None
#C525 Ni	0.5 gms.	Rough-polished sapphire disc	111.6	1619	Surface condition
#C525 Ni	0.75 gms.	Fine-polished sapphire disc	112.4	1650	Drop size
#C525 Ni	0.5 gms.	Sintered alumina pdr. (600mesh)	119.4	1846	Orientation and surface condition
Ni + 9.3% Ti	0.5 gms.	Fine-polished sapphire disc	80.1	623	None
Ni + 10% Ti	0.5 gms.	Sintered alumina pdr. (600 mesh)	79.1	591	Orientation and surface condition
High purity Ni	0.5 gms.	Fine-polished sapphire disc	113.7	1581	Metal purity
Carbonyl Ni	0.5 gms.	Fine-polished sapphire disc	104.1	1360	Metal purity

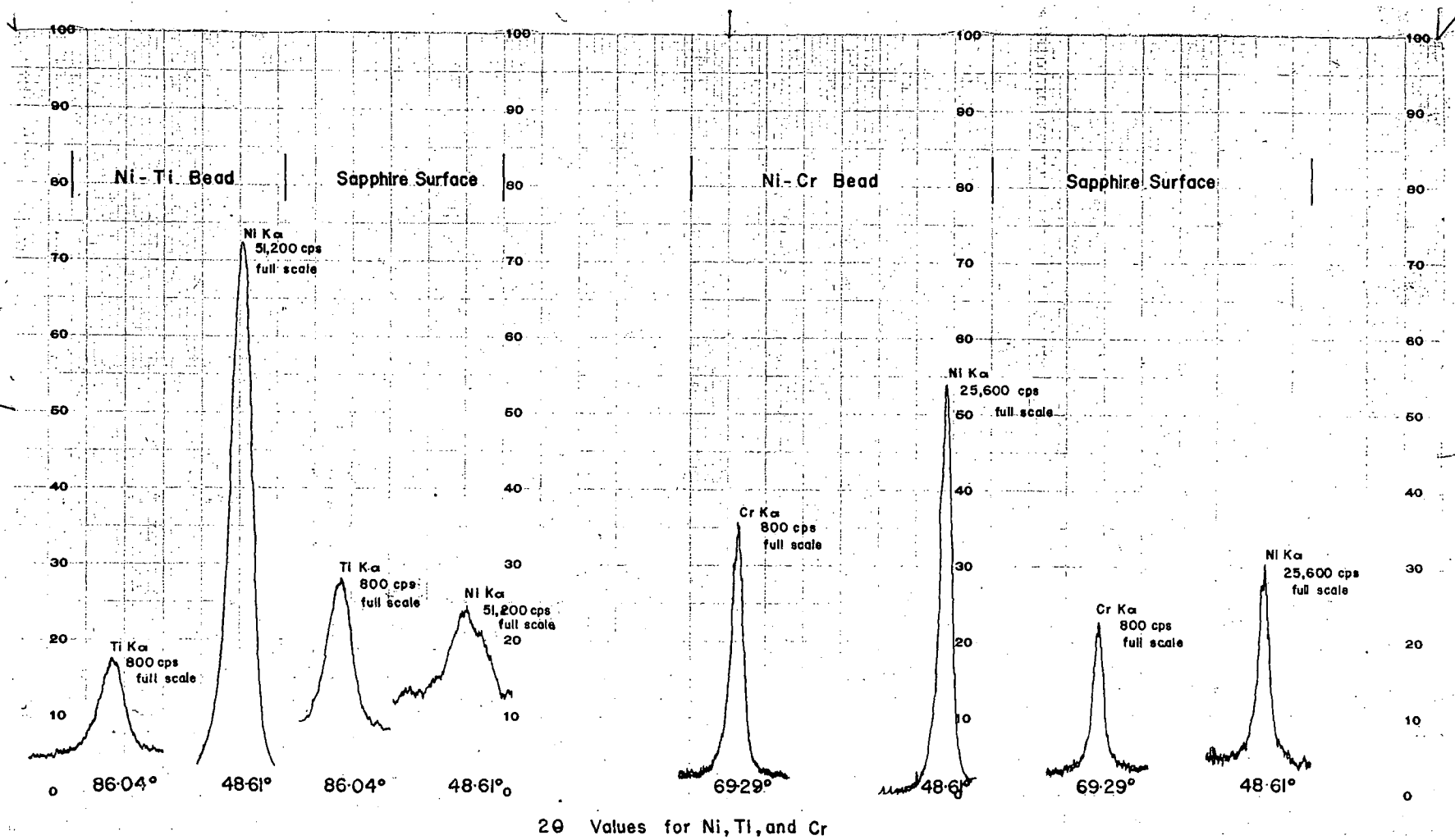


Figure 16. X-ray fluorescence curves.

concentrations.

Although this method is inherently inaccurate for absolute values if the samples are not standardized, the relative values for any one X-ray specimen are significant. After correcting the curves for sensitivity and scale factors of the counter, ratios of the metals in the drop and on the sapphire can be obtained. These approximate ratios are shown in Table IV. Unfortunately, this method gives the relative amounts of the elements but no indication of the form in which the elements exist.

TABLE IV  
X-ray Fluorescence Analysis

Alloy Composition	Composition Ratio after Test	
	In Metal Drop	On Sapphire Surfaces
Ni + 2.1 Ti	$\frac{\text{Ni}}{\text{Ti}} = \frac{47}{1}$	$\frac{\text{Ni}}{\text{Ti}} = \frac{0.1}{1}$
Ni + 10% Cr	$\frac{\text{Ni}}{\text{Cr}} = \frac{9}{1}$	$\frac{\text{Ni}}{\text{Cr}} = \frac{0.2}{1}$

## 2. Debye-Scherrer Powder Patterns.

During the heating cycle in the nickel-titanium and nickel-chromium experiments, colored interfacial layers formed between the alloys and sapphire. Nickel-titanium alloys produced a blue-black film on the portion of the sapphire surface covered by the metal drop. Variations in temperature about the melting point of the alloy caused this blue-black film to flake off the sapphire. Nickel-

chromium alloys, on the other hand, produced a pale green material at the interface. This material was not a film but appeared to be a diffusion layer which was physically inseparable from the underlying sapphire.

The blue-black flakes from the nickel-titanium experiments were cleaned and powdered in preparation for X-ray diffraction in a Debye-Scherrer camera. Preliminary calculations on the resulting powder patterns indicated that the interfacial film was the reaction product, alpha titanium sesqui oxide ( $\alpha\text{-Ti}_2\text{O}_3$ ). Because the recorded data for this material in the A.S.T.M. card index was incomplete, further calculations were necessary to positively identify the material as being  $\alpha\text{-Ti}_2\text{O}_3$ . The X-ray powder patterns were subsequently indexed by the use of the extinction rules for  $\alpha\text{-Ti}_2\text{O}_3$  and the Bunn chart for hexagonal materials. The details of these calculations have been included in Appendix III. The calculated and observed results were in close enough agreement to prove that the material was  $\alpha\text{-Ti}_2\text{O}_3$ . The pertinent data, which was tabulated and submitted to the Joint Committee on Chemical Analysis by Powder Diffraction Methods, was accepted for publication in the card index.

A technique for the separation of the green, interfacial layer formed in the nickel-chromium experiments from the underlying sapphire was not discovered. Powder samples of the combined material and a sample of pure sapphire were, therefore, prepared for X-ray diffraction. Because the green interfacial material was previously reported<sup>2,3,26</sup> to be a solid solution of  $\text{Cr}_2\text{O}_3$  in  $\text{Al}_2\text{O}_3$ , a known solid solution of this type was X-rayed in a similar

manner for use as a reference. The details of the resulting powder patterns are presented in Appendix IV.

If the interfacial layer were a solid solution of  $\text{Cr}_2\text{O}_3$  in  $\text{Al}_2\text{O}_3$ , the powder pattern of the layer would be similar to the pattern of the major components. This was not the case. Films showed strong  $\text{Al}_2\text{O}_3$  lines along with a very weak pattern of an unknown material. Although this weak pattern could not be identified, it was concluded that the interfacial layer consisted of a compound or compounds and possibly a solid solution. The diffraction pattern of the unknown material did not correspond exactly to any of the recorded patterns for the oxides of chromium.

### C. Thermodynamic Calculations.

Assuming that the nickel-titanium and nickel-chromium alloys are ideal solutions (the activity coefficients are unity and the heats of mixing are zero), the Gibbs adsorption equation can be applied to these alloys.<sup>33</sup> The excess surface concentration of the solute,  $\Gamma$ , is given by:

$$\Gamma = \frac{-d\gamma}{RT \, d \ln c} \quad (6)$$

where  $\gamma$  is the surface energy,  $R$  is the gas constant,  $T$  is the absolute temperature and,  $c$  is the bulk concentration of the solute. Because small additions of titanium (less than 10% Ti) and chromium (less than 19% Cr) have no measurable effect on the liquid surface energy, the excess concentrations of titanium and chromium at the liquid-vapour interface are zero. Similar additions do show a marked effect on the solid-liquid interfacial energy in the composition ranges of 1 to 2 percent titanium and

6 to 12 percent chromium (see Figures 14 and 15). Application of equation (6) in these ranges indicates excess solute concentrations of  $24.5 \times 10^{14}$  Ti atoms per  $\text{cm.}^2$  and  $40.7 \times 10^{14}$  Cr atoms per  $\text{cm.}^2$  at the interface (see Appendix V). These surface excess values refer to the number of solute atoms at the interface above the number in the liquid alloy.

The extent to which the excess titanium and chromium at the interface react with the sapphire to form oxides of these metals can be predicted from thermodynamic data.<sup>10,11</sup> Although the free energy for the reaction,  $\text{Al}_2\text{O}_3 + 2 \text{Ti} \rightarrow \text{Ti}_2\text{O}_3 + 2 \text{Al}$ , is positive, the equilibrium constant is sufficiently large that a noticeable reaction can be predicted (see Appendix V). The free energy for the reaction,  $\text{Al}_2\text{O}_3 + 2 \text{Cr} \rightarrow \text{Cr}_2\text{O}_3 + 2 \text{Al}$ , is similarly positive, but the very low value of the equilibrium constant indicates only a very slight reaction (see Appendix V).

#### IV. DISCUSSION AND CONCLUSIONS

##### A. Discussion of Results.

The surface energy of liquid nickel is not affected greatly by additions of titanium and chromium<sup>12,13</sup> but it is markedly changed by the presence of minor surface-active impurities.<sup>15</sup> The surface energies of the three grades of nickel used in the work varied as much as 15 percent. The variations, however, could not be related to a specific impurity on the basis of the experimental values.

On the other hand, the interfacial energy between nickel alloys and alumina is affected by the surface condition of the alumina, the crystallographic orientation of the alumina crystals, and the composition of the metal drop. Because these effects are additive, the effect of alloy additions to nickel was measured by maintaining constant surface conditions and crystal orientation. Experimental values showed a decrease in interfacial energy with increasing solute concentration. Because the scatter of the results was so great, especially in the higher alloy compositions, difficulties in establishing the curves of best fit were encountered (see Figures 14 and 15). This scatter was believed to be caused by inhomogeneous mixing of the metal powders in the compact. Regardless of the scatter, however, the interfacial energies show a marked decrease within a very narrow composition range.

The decrease in interfacial energy with increasing bulk concentration of the solute in the nickel alloys has been

attributed to the selective adsorption of the solute atoms at the interface<sup>12,13,17</sup>. The rapid decrease in interfacial energy above a critical bulk concentration is caused by the adsorption of the solute in a complete monolayer at the interface. The constant slope in a narrow range above the critical concentration indicates that the interfacial solute concentration remains constant (at the monolayer concentration) throughout the range. At higher concentrations, the interfacial energy reaches a nearly constant value which presumably corresponds to the multilayer adsorption of solute atoms.

The theoretical concentration of titanium atoms in a close-packed plane is  $12 \times 10^{14}$  atoms per  $\text{cm.}^2$ <sup>12</sup> Application of the Gibbs' adsorption equation to the experimental curve for the nickel-titanium alloys of this investigation indicates a titanium excess concentration of  $24.5 \times 10^{14}$  atoms per  $\text{cm.}^2$  at the interface. Although this concentration is physically impossible, it does show that at least a close-packed monolayer is completed at 1.1 percent titanium (the concentration at which the constant slope begins). Similarly, the experimental value for the excess concentration of chromium in the constant-slope range ( $40.7 \times 10^{14}$  Cr atoms per  $\text{cm.}^2$ )<sup>13</sup> indicates that at least a monolayer of chromium ( $13 \times 10^{14}$  atoms per  $\text{cm.}^2$ )<sup>13</sup> is completed at approximately 6 percent chromium. Because the experimental excess concentrations disagree with the monolayer concentrations, the theoretical slopes were calculated from the Gibbs' equation for monolayers of titanium and chromium. These slopes have been drawn on the graphs (Figures 14 and 15) as dotted lines.

The noticeable differences in the experimental and theoretical slopes for both titanium and chromium could be due to errors in the experimental values or due to assumptions required to apply the theory. The differences could be partially caused by the scatter of experimental points resulting in incorrect positioning of the curve on the graph.

Regardless of the disagreement between the experimental and theoretical slopes, the concentrations at which interfacial energy decreases rapidly with increasing solute concentration are approximately 1.1 percent titanium and 6 percent chromium. All X-ray analyses were made on samples containing higher solute concentrations. Thus, significant amounts of adsorption would be expected in these samples.

The selective adsorption of both titanium and chromium at the metal-sapphire interface was definitely detected in the X-ray fluorescence analyses. Although precise quantitative analyses of only a few atom layers are impossible by this method, the results did indicate a much higher ratio of titanium or chromium to nickel on the surface of the sapphire than in the original alloy.

From thermodynamic calculations, a limited reaction between the excess titanium at the interface and the underlying sapphire is predicted. By X-ray diffraction, a reaction product was shown to be  $\alpha$ -Ti<sub>2</sub>O<sub>3</sub>. The oxygen atoms for the reaction lie in the  $\langle 10\bar{1}2 \rangle$  planes of the Al<sub>2</sub>O<sub>3</sub> lattice. The concentration of oxygen atoms in this plane is one-thirteenth the concentration

in the basal plane ( $15.3 \times 10^{14}$  oxygen atoms per  $\text{cm.}^2$ ).<sup>17</sup> However, thirteen  $\langle 10\bar{1}2 \rangle$  planes are at least partially exposed to the surface. The effective concentration of oxygen atoms at the surface of a  $\langle 10\bar{1}2 \rangle$  plane is, therefore, approximately the same as the concentration in the basal plane. To satisfy the titanium-oxygen ratio for the formation of  $\alpha\text{-Ti}_2\text{O}_3$ , approximately  $10 \times 10^{14}$  titanium atoms would tend to concentrate at the interface. This is less than a close-packed monolayer. Further reaction of the titanium and alumina would involve the diffusion of titanium atoms from the interface into the alumina lattice and the diffusion of freed aluminum atoms from the alumina into the metal. The reaction would continue until the activity of the titanium in the metal drop was reduced to a value at which a monolayer of titanium would not form, or until the activity of the aluminum in the metal drop was high enough for a significant back-reaction. For bulk concentrations well above the critical concentration required for the formation of a monolayer, reaction layers several atom layers in thickness would be expected to form. This was the case. The interfacial layers of  $\alpha\text{-Ti}_2\text{O}_3$  were of visible thicknesses.

The reaction product,  $\alpha\text{-Ti}_2\text{O}_3$ , and the sapphire plaques,  $\alpha\text{-Al}_2\text{O}_3$ , have similar crystallographic properties. Both materials are in the rhombohedral division of the hexagonal system and both are in the  $D_{3d}^6 R\bar{3}c$  space group. The unit axis length and axial angle for  $\alpha\text{-Ti}_2\text{O}_3$  are  $a_0 = 5.42 \text{ \AA}$  and  $\alpha = 56^\circ 32'$  and for  $\alpha\text{-Al}_2\text{O}_3$  are  $a_0 = 5.12 \text{ \AA}$  and  $\alpha = 55^\circ 17'$ . Thus, the structure of  $\alpha\text{-Ti}_2\text{O}_3$  is compatible with both the sapphire and the adsorbed titanium.

The adsorbed chromium atoms would similarly be expected

to produce a significant amount of reaction product. Although thermodynamic calculations do not predict any more than a very limited reaction between chromium and alumina, the reaction would proceed to approximately the same point as the titanium-alumina reaction if the reaction product, aluminum, were again removed from the reacting layer. Assuming that the chromium-alumina reaction is one of simple replacement of aluminum in the alumina lattice by chromium, the oxide product would form in a structure similar to alumina. The chromium oxide structure which closely resembles the alumina structure is that of  $\text{Cr}_2\text{O}_3$  (see Figure 21, Appendix IV). The  $\text{Cr}_2\text{O}_3$  would also be compatible with both the alumina lattice and the adsorbed metal at the interface. However, the chromium-alumina reaction layer was not positively identified.

The reaction of nickel-zirconium alloys with alumina appeared to be violent and an oxide scale formed on the metal drop. Zirconium probably segregated at the interface and reacted with the alumina as in the cases of titanium and chromium. The oxide product formed by the reaction, however, must have been incompatible with the alumina lattice to such an extent to cause it to spall off the surface of the alumina and gather on the surface of the liquid metal.

## B. Conclusions.

Bond formation between single crystals of alumina and nickel alloys involves two basic mechanisms - the formation of an excess solute concentration at the metal-ceramic interface, and a reaction between these excess atoms and the alumina. The two

mechanisms were studied with two different approaches - measurement of interfacial energies between the metal and ceramic by the sessile-drop method, and analysis of the bonded interfaces by X-ray techniques.

The decrease in the metal-alumina interfacial energy with increasing concentrations of titanium and chromium in nickel is a result of the selective adsorption of titanium and chromium atoms at the interface. The most significant decrease occurs when the interface is saturated with adsorbed atoms. Saturation occurs at approximately 1.1 percent titanium and 6 percent chromium in nickel. At higher concentrations of titanium and chromium, the interfacial energy remains approximately constant with alloy composition. This is attributed to three-dimensional saturation of the interface.

X-ray fluorescence analyses of the alumina surfaces and nickel alloys indicated semi-quantitatively that titanium and chromium segregate at the metal-ceramic interface. However, the form in which the adsorbed atoms exist at the interface cannot be determined by this method.

X-ray diffraction data showed conclusively that the adsorbed titanium and chromium atoms reacted with the alumina at the interface to form new compounds. For nickel-titanium alloys on alumina, the reaction product,  $\alpha$ -Ti<sub>2</sub>O<sub>3</sub>, was positively identified. This compound is crystallographically compatible with the alumina lattice and the adsorbed titanium atoms at the interface. From a similar study of nickel-chromium on alumina,

one would expect the formation of  $\text{Cr}_2\text{O}_3$ . The reaction product, however, could not be identified but it was concluded that compound formation did occur at the interface. With the assumption that the reactions of both titanium and chromium with alumina occur by simple replacement of the aluminum, the relatively thick experimental reaction layers on the alumina surface can be predicted from adsorption calculations.

A limited study of nickel-zirconium alloys on alumina indicated a violent reaction between the zirconium and alumina. Quantitative measurements of interfacial energies and identification of the reaction products were impossible.

## V. RECOMMENDATIONS FOR FURTHER WORK

In this investigation, the mechanisms of bond formation were thoroughly investigated for only two metal-ceramic systems. As mentioned previously, the original purpose of this investigation was to study the bond between single crystals of sapphire and a number of nickel alloys. Because of experimental difficulties, additions of manganese, iron, vanadium, molybdenum, gallium, bismuth, tantalum and columbium were not attempted. With these difficulties now eliminated, it would be interesting to complete the study to establish the bond mechanisms which are common to all similar systems. It appears that X-ray techniques are most promising for the development of general rules for the selection of metal-ceramic combinations with optimum properties.

APPENDIX IDrying Agents

The common drying agents and their respective drying powers are listed in Table V. Silica gel, anhydrous  $\text{CaSO}_4$  and  $\text{P}_2\text{O}_5$  were used in this work to extract water from hydrogen gas.

TABLE V  
Drying Agents and Drying Powers

<u>Material</u>	<u>MgH<sub>2</sub>O/liter of gas</u>
$\text{CuSO}_4$ (granular)	2.8
$\text{CaCl}_2$ (anhydrous)	1.5
$\text{CaCl}_2$ (fused)	1.25
$\text{ZnCl}_2$ (anhydrous)	0.9
$\text{Ba}(\text{ClO}_4)_2$ (anhydrous)	0.8
$\text{NaOH}$ (sticks)	0.35
$\text{CaCl}_2$ (dehyd.)	0.20
$\text{CaBr}_2$	0.15
$\text{B}_2\text{O}_3$	0.032
$\text{MgClO}_4 \cdot 3\text{H}_2\text{O}$	0.03
Silica gel	0.014
$\text{KOH}$ (sticks)	0.008
$\text{MgO}$	0.008
$\text{Al}_2\text{O}_3$	0.005
$\text{CaSO}_4$ (anhydrous)	0.005
$\text{H}_2\text{SO}_4$ (conc.)	0.005
$\text{CaO}$	0.003
$\text{Mg}(\text{ClO}_4)_2$ (anhydrous)	0.002
$\text{BaO}$	0.0007
$\text{P}_2\text{O}_5$	0.0002

APPENDIX II

Calculations on Sessile-Drop Measurements.

Calculations of surface tensions and contact angles can be made from sessile-drop dimensions using the Bashforth and Adams tables.<sup>4</sup> These tables have been derived from the mathematics of the equilibrium forces of surface tension tending to form a spherical surface and of gravity tending to flatten the drop. The methods of calculation are presented in detail by Ellefson and Taylor.<sup>5,6</sup> Sample calculations for both methods used in this investigation are given below:

Example I. For obtuse contact angles<sup>5</sup>

Consider the measurements (see Figure 11) on a sessile drop of Sherritt #C525 Ni.

$$X = .3208 \text{ cm.} \quad X^1 = .3109 \text{ cm.}$$

$$Z = .2951 \text{ cm.} \quad Z^1 = .3603 \text{ cm.}$$

$$\text{Therefore } \frac{X}{Z} = 1.0871$$

Reference is now made to the Bashforth and Adams' table which relates values of  $\beta$  and  $\frac{X}{Z}$ . These  $\beta$  -values are related to surface tension by the following equation:

$$\beta = \frac{g \delta b^2}{\gamma_{LV}} \quad (7)$$

where  $g$  = the acceleration due to gravity

$\delta$  = the density of the liquid

$b$  = the radius of curvature of the apex of the drop

$\gamma_{LV}$  = the surface tension of the liquid

By interpolation, the following value is obtained:

$$\beta = 0.4723$$

By using this  $\beta$ -value in reference to a second Table relating to  $\frac{X}{b}$  and  $\frac{Z}{b}$  at  $\phi = 90$  degrees, it is possible to obtain the following values by interpolation:

$$\frac{X}{b_x} = 0.93604, \text{ therefore } b_x = 0.3427 \text{ cm.}$$

$$\text{and } \frac{Z}{b_z} = 0.86147, \text{ therefore } b_z = 0.3425 \text{ cm.}$$

The mean value of the radius of curvature of the apex of the drop is, therefore  $b = 0.3426$  cm.

The surface tension can then be calculated from Equation (7):

$$\gamma_{LV} = 1848 \text{ dynes per cm.}^2$$

where the density of molten nickel<sup>19</sup> is 7.6 gms. per cm.<sup>3</sup> and the acceleration due to gravity is 980.7 cm. per sec.<sup>2</sup>.

To obtain the contact angle, the reverse procedure is used:

$$\frac{X}{b} = 0.3426 \qquad \frac{Z}{b} = 0.9074$$

Referring to the second Table again, the angles given by the  $\frac{X}{b}$  and  $\frac{Z}{b}$  values at  $\beta = 0.4734$  can be obtained by interpolation:

$$\phi_x = 106.2^\circ \qquad \phi_z = 105.2^\circ$$

The mean angle, 105.7, is equal to  $\theta$ , the contact angle.

A calculated value of the interfacial energy can then be obtained from Equation (1), if the surface energy of the solid ceramic is known.

Example II. For acute contact angles.<sup>6</sup>

Assuming that the drop is small enough that the drop shape is a true spherical segment, the contact angle is given by (see Figure 11):

$$\theta = 2 \tan^{-1} \frac{Z^1}{X^1} \quad (8)$$

Consider the experimental values for Ni + 19% Cr on sapphire:

$$X^1 = 0.317 \text{ cms.}$$

$$Z^1 = 0.276 \text{ cms.}$$

From Equation (8), therefore,  $\theta = 82.1^\circ$

APPENDIX III

Detailed Calculations on  $\alpha$ -Ti<sub>2</sub>O<sub>3</sub> Powder Patterns

Figure 17 is a photographic print of a typical X-ray powder pattern produced from a sample of interfacial material from the nickel-titanium experiments. Table VI shows the

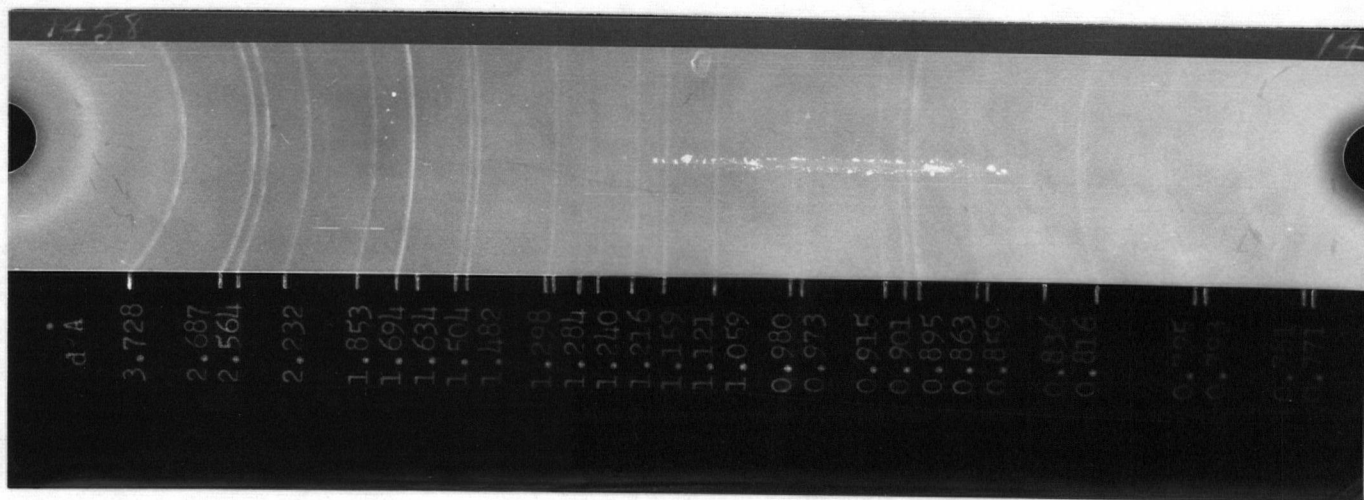


Figure 17. X-ray powder pattern No. 1458 of interfacial material in Ni-Ti experiments.

preliminary data obtained from the pattern. The tabulated d-values and line intensities compare to those recorded in the A.S.T.M. X-ray Card Index for alpha titanium sesqui oxide (see Figure 18). However, the data on this card is incomplete. For positive identification of the interfacial material, further calculations on the observed data were necessary. These calculations are outlined below:

From Figure 18, the rhombohedral indices for  $\alpha$ -Ti<sub>2</sub>O<sub>3</sub> are:

$$a_0 = 5.42 \text{ \AA} \quad \text{and} \quad \alpha = 56^\circ 32'$$



These rhombohedral values can be expressed in terms of hexagonal values by the use of the following equations:<sup>35</sup>

$$\sin \frac{\alpha}{2} = \frac{3}{2\sqrt{3 + (c/a)^2}} \quad (9)$$

$$a_0 = \frac{1}{\sqrt{3}} \sqrt{3a^2 + c^2} \quad (10)$$

The equivalent hexagonal unit cell dimensions are:

$$a = 5.14 \text{ \AA} \quad \text{and} \quad c = 13.61 \text{ \AA}$$

Therefore,  $c/a = 2.648$  and  $\log c/a = 0.4229$ . From the Bunn chart for hexagonal materials, all the possible low-index planes for  $\alpha\text{-Ti}_2\text{O}_3$  are obtained. Only the planes with indices that obey the extinction rules for  $\alpha\text{-Ti}_2\text{O}_3$  (see Table VII) can diffract X-rays. These indices can then be used to obtain calcu-

TABLE VII  
Extinction Rules<sup>36</sup> for Space Group  $D_{3d}^6 R\bar{3}c$

Plane	required (n=integer)
hki $\bar{l}$	$h + i + \bar{l}$ must equal $3n$
h0 $\bar{h}l$	$h + i + \bar{l} = 3n$ and $\bar{l} = 2n$
hh $2\bar{h}l$	$h + i + \bar{l} = 3n$
000 $\bar{l}$	Sum 6

lated d-values for the respective planes from the following formula:<sup>35</sup>

$$\frac{1}{d^2} = \frac{4}{3} \frac{h^2 + k^2 + \bar{l}^2}{a^2} + \frac{\bar{l}^2}{c^2} \quad (11)$$

These calculated d-values should agree with the observed d-values obtained from the powder pattern if the specimen is  $\alpha\text{-Ti}_2\text{O}_3$  (see Table VIII).

TABLE VIII

Calculated and Observed Data for Film No. 1458

$d\overset{\circ}{A}$ (obs'd.)	I/I <sub>1</sub>	Rhomb. Index	$d\overset{\circ}{A}$ (calc'd.)
3.728	50	110	3.725
2.687	60	211	2.700
2.564	60	101	2.569
2.232	40	210	2.236
1.853	40	220	1.862
1.694	100	321	1.700
1.634	2	211	1.633
1.504	40	310	1.507
1.482	40	211	1.483
1.298	20	433      432	1.302      1.304
1.284	10	202	1.285
1.240	8	411	1.241
1.216	5	301	1.215
1.159	30	442      321	1.161      1.160
1.121	30	410      420	1.124      1.118
1.059	30	532      400	1.058      1.057
.980	5	531      411	.979      .978
.973	5	312	.971
.915	20	541	.914
.901	20	633	.901
.895	20	510	.893
.863	5	332	.861
.859	5	654      303	.856      .856
.836	3	655      402	.836      .835
.816	10	422	.816
.795	5	664	.795
.793	5	323	.794
.781	3	501	.778
.771	3	531	.772

The hexagonal indices (hkℓ) used in the above calculations can be corresponding rhombohedral indices (HKL) by the following formulae:<sup>34</sup>

$$H = 1/3(2h + k + \ell) \quad (12)$$

$$K = 1/3(-h + k + \ell) \quad (13)$$

$$L = 1/3(-h - 2k + \ell) \quad (14)$$

The rhombohedral indices have been listed in Table VIII. Thus, the powder pattern has been completely indexed and the material has been identified as  $\alpha$ -Ti<sub>2</sub>O<sub>3</sub>.

APPENDIX IV.X-ray Diffraction Data from Ni-Cr Experiments.

Photographic prints of X-ray powder patterns produced by samples of sapphire, sapphire mixed with the interfacial layer of the Ni-Cr experiments, and a solid solution of  $\text{Cr}_2\text{O}_3$  in  $\text{Al}_2\text{O}_3$  are shown in Figure 19.

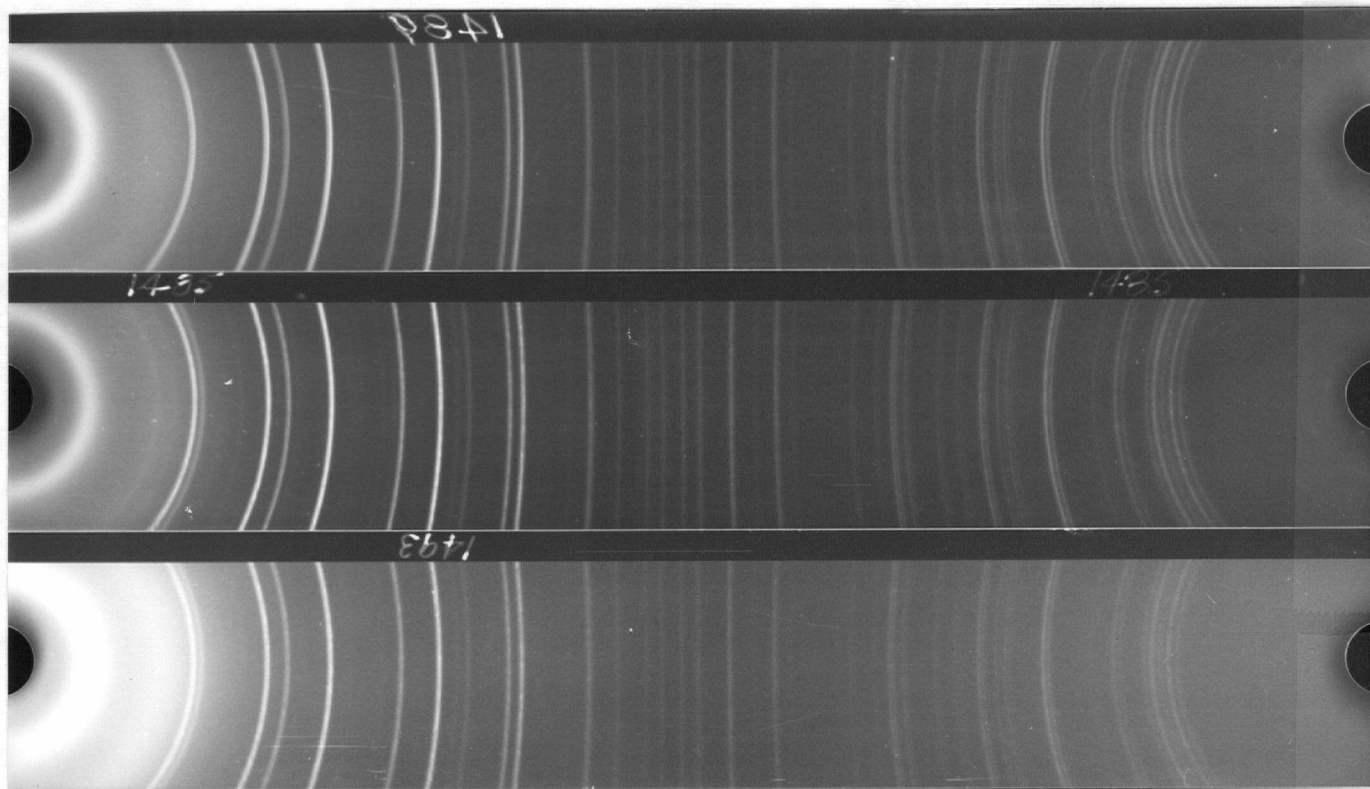


Figure 19. X-ray powder patterns, Nos. 1489, 1485 and 1493. (Top - Pure  $\text{Al}_2\text{O}_3$ , Middle -  $\text{Al}_2\text{O}_3$  and unknown, Bottom - Solid solution of  $\text{Cr}_2\text{O}_3$  in  $\text{Al}_2\text{O}_3$ ).

The observed X-ray data for the mixture of the unknown material and sapphire are listed in Table IX. The reported d-values for  $\text{Al}_2\text{O}_3$  given in the A.S.T.M. Card Index are shown in Figure 20. The d-values in Table IX, which do not appear in Figure 20, are undoubtedly due to the presence of the interfacial layer in the specimen. These d-values have been starred (\*) in

TABLE IX

Data from Film No. 1485

Line No.	I/I <sub>1</sub>	d <sup>o</sup> dÅ(obs'd.)	Line No.	I/I <sub>1</sub>	d <sup>o</sup> dÅ(obs'd.)
1	20	4.244 彗	25	30	1.187
2	20	3.871 彗	26	30	1.145
3	80	3.474	27	30	1.122
4	50	彗 3.342 彗	28	30	1.096
5	20	2.801 彗	29	30	1.076
6	10	2.607 彗	30	50	1.043
7	100	2.545	31	10	1.016
8	80	2.376	32	40	.998
9	10	2.311 彗	33	10	.980
10	100	2.078	34	20	.935
11	10	1.953 彗	35	10	.917
12	10	1.926 彗	36	40	.908
13	10	1.814 彗	37	30	.899
14	10	1.766 彗	38	20	.881
15	80	1.737	39	10	.869
16	100	1.597	40	30	.858
17	20	1.541	41	20	.850
18	40	1.507	42	10	.846 彗
19	80	1.400	43	50	.830
20	90	1.372	44	10	.814
21	10	1.335 彗	45	30	.807
22	10	1.272	46	20	.799 彗
23	10	1.254 彗	47	20	.797 彗
24	40	1.236	48	20	.793 彗

5-0712

d	2.09	2.55	1.60	3.479	α-Al <sub>2</sub> O <sub>3</sub>						
I/I <sub>1</sub>	100	92	81	74	ALPHA ALUMINUM OXIDE			CORUNDUM			
Rad. Cu	λ 1.5405				Filter	d Å	I/I <sub>1</sub>	hkl	d Å	I/I <sub>1</sub>	hkl
Dist.	Cut off				Coll.	3.479	74	102	1.0791	7	214
I/I <sub>1</sub>	d corr. abs?				2.552	92	014	1.0426	13	226	
Ref. SWANSON AND FUYAT, IBS CIRCULAR 53, Vol. II	20° (1952)				2.379	42	110	1.0175	1	402	
Sys. HEXAGONAL	SG. D <sub>3h</sub> - R3c				2.155	41	006	0.9976	11	1,2,10	
a	12.991 Å				1.740	43	204	.9345	3	138	
c	Z 6				1.601	81	116	.9178	2	229	
Ref. IBID.					1.546	3	121	.9076	12	234	
ε <sub>a</sub>	news				1.510	7	109	.9052	3	1,0,14	
2V	D <sub>3</sub> 987 mp				1.404	32	134	.8991	6	410	
Ref.	Color				1.274	49	300	.8804	4	413	
					1.276	2	028	.8698	2	408	
					1.239	16	0,1,10	.8580	12	3,1,10	
					1.1898	6	320	.8502	4	3,0,12	
					1.1701	41	306	.8303	22	416	
					1.1470	4	223	.8137	4	1,1,15	
					1.1382	1	311	.8075	11	0,4,10	
					1.1254	5	132				
					1.0988	6	2,0,10				
					1.0831	3	0,0,12				

SAMPLE FROM MALLINCKRODT CHEM. WORKS. SPECT.  
ANAL.: <0.1% K, Na, Si; <0.01% Ca, Cu, Fe, Mg, Pb;  
<0.001% B, Cr, Li, Mn, Ni.  
X-RAY PATTERN AT 26°C  
REPLACES 1-1243, 1-1296, 2-1227, 2-1373, 3-1033

Figure 20. A.S.T.M. Card No. 5-0712 for α-Al<sub>2</sub>O<sub>3</sub>

Table IX. The same lines are missing from the  $\text{Cr}_2\text{O}_3\text{-Al}_2\text{O}_3$  solid solution pattern except for line No.4. Hence, the extra lines are not due to the presence of a  $\text{Cr}_2\text{O}_2\text{-Al}_2\text{O}_3$  solution. A compound with a definite crystal structure must form at the interface.

From previous experience with the Ni-Ti alloys, the expected compound would be  $\text{Cr}_2\text{O}_3$  because it has similar crystallographic properties. However, the extra lines do not correspond to lines of  $\text{Cr}_2\text{O}_3$  (see Figure 21). Other materials, especially the

6-0504									
d	2.67	2.48	1.67	3.633	$\text{Cr}_2\text{O}_3$ ★				
I/I <sub>1</sub>	100	96	90	74	CHROMIUM (III) OXIDE				
Rad. Cu	λ 1.5405	Filter							
Dia.	Cut off	Coll.							
I/I <sub>1</sub>		d corr. abs.?	d Å	I/I <sub>1</sub>	hkl	d Å	I/I <sub>1</sub>	hkl	
Ref. SWANSON ET AL., NBS CIRCULAR 539 Vol. I (1955)			3.633	74	012	0.9370	12	410	
			2.666	100	104	.8957	14	1.3.10	
			2.490	96	110	.8683	7	3.0.12	
			2.264	12	006	.8658	23	416	
			2.176	38	113	.8425	8	4.0.10	
Syn. HEXAGONAL	S.G. $D_{6h} - R\bar{3}c$		2.048	9	202	.8331	11	1.0.16	
a 4.954	b <sub>c</sub> 13.584	A C	1.8156	39	024	.8263	9	330	
Ref. I.B.D.	β γ	Z 6	1.672	90	116	.7977	15	3.2.10	
			1.579	13	122				
			1.465	25	214				
ε a	n=β	ξ γ	1.4314	40	300				
2V	Dx5.23 mp	Color	1.2961	20	1.0.10				
Ref.			1.2398	17	220				
			1.2101	7	306				
SAMPLE FROM JOHNSON, MATTHEY AND CO. LTD.			1.1731	14	128,312				
SPECT. ANAL. <0.001% Ca, Mn <0.0001% Si, Cu.			1.1488	10	0.2.10				
X-RAY PATTERN AT 26°C. $\text{Fe}_2\text{O}_3$ STRUCTURE TYPE.			1.1239	10	134				
			1.0874	17	226				
			1.0422	16	2.1.10				
REPLACES 1-1294, 2-1362, 3-1124, 4-0765			0.9462	13	324				

Figure 21. A.S.T.M. Card No.6-0504 for  $\text{Cr}_2\text{O}_3$

oxides of chromium, were similarly investigated but all the extra lines could not be identified with any one material. This could be due to the low intensity of the lines and the resulting errors in calculations of d-values or to the presence of more than one compound in the unknown material.

APPENDIX VThermodynamic Calculations.(a) Application of Gibbs' adsorption equation.

From Figure 14,

At, 1.3% Ti,  $\gamma_{SL} = 1060$  ergs per  $\text{cm.}^2$

and at 2.0% Ti,  $\gamma_{SL} = 800$  ergs per  $\text{cm.}^2$

Therefore,  $d \ln c = 0.433$  and  $d \gamma_{SL} = -260$  ergs per  $\text{cm.}^2$   
or  $-621 \times 10^{-8}$  gram-calories per  $\text{cm.}^2$ . Applying the  
Gibbs' equation at  $T = 1773^\circ\text{K}$ ,

$$\begin{aligned} \Gamma &= \frac{-(-621 \times 10^{-8})}{(2)(1773)(0.433)} \text{ moles per cm.}^2 \\ &= (4.05 \times 10^{-9})(6.06 \times 10^{23}) \text{ Ti atoms per cm.}^2 \\ &= 24.5 \times 10^{14} \text{ Ti atoms per cm.}^2 \end{aligned}$$

From Figure 15,

At 7.4% Cr,  $\gamma_{SL} = 1240$  ergs  $\text{cm.}^2$

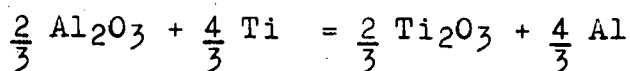
and at 10.0% Cr,  $\gamma_{SL} = 940$  ergs per  $\text{cm.}^2$

Therefore,  $d \ln c = 0.301$  and  $d \gamma_{SL} = -300$  ergs per  $\text{cm.}^2$   
or  $-717 \times 10^{-8}$  gram-calories per  $\text{cm.}^2$ . Applying the  
Gibbs' equation at  $T = 1773^\circ\text{K}$ ,

$$\begin{aligned} \Gamma &= \frac{-(-717 \times 10^{-8})}{2(1773)(0.301)} \text{ moles per cm.}^2 \\ &= (6.71 \times 10^{-9})(6.06 \times 10^{23}) \text{ Cr atoms per cm.}^2 \\ &= 40.7 \times 10^{14} \text{ Cr atoms per cm.}^2 \end{aligned}$$

(b) Reaction Calculations.

For the Ti-Al<sub>2</sub>O<sub>3</sub> reaction at 1500°C.

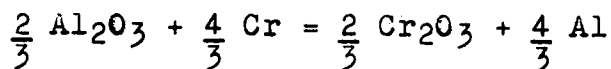


$$\begin{aligned} \Delta F_{\text{rxn}} &= (-163) - (-176) \text{ kcal per mole O}_2 \\ &= 13,000 \text{ cal per mole O}_2 \end{aligned}$$

$$\ln K = \frac{-\Delta F}{RT} = \frac{-13,000}{2(1773)} = -3.67$$

Therefore, the equilibrium constant,  $K = 2.5 \times 10^{-2}$

For the Cr-Al<sub>2</sub>O<sub>3</sub> reaction at 1500°C.



$$\begin{aligned} \Delta F_{\text{rxn}} &= (-103) - (-176) \text{ kcal per mole O}_2 \\ &= 73,000 \text{ cal per mole O}_2 \end{aligned}$$

$$\ln K = \frac{-\Delta F}{RT} = \frac{-73,000}{2(1773)} = -20.6$$

Therefore, the equilibrium constant,  $K = 1 \times 10^{-9}$

APPENDIX VI

Evaluation of Experimental Errors in Sessile-drop Calculations.

$$\gamma_{SL} = \gamma_{SV} - \gamma_{LV} \cos \theta$$

- (1) Error in temperature =  $\pm 5^{\circ}\text{C}$

Therefore, resulting experimental errors are:

$$\gamma_{SV} = \pm 0.5 \text{ ergs/cm.}^2$$

$$\gamma_{LV} = \pm 5.0 \text{ ergs/cm.}^2$$

and,  $\gamma_{SL} = \pm 5.5 \text{ ergs/cm.}^2$

- (2) Error in sessile-drop measurements =  $\pm .00254 \text{ cm.}$

Resulting experimental errors are:

$$\gamma_{LV} = \pm 2 \text{ ergs/cm.}^2$$

$$\theta = \pm 0.1^{\circ}$$

Error factor for drop size<sup>31</sup> = 10

Therefore,

$$\gamma_{LV} = \pm 20 \text{ ergs/cm.}^2$$

$$\theta = \pm 1^{\circ}\text{C}$$

and,  $\gamma_{SL} = \pm 40 \text{ ergs/cm.}^2$

- (3) Total resulting experimental error in

$$\gamma_{SL} = \pm 45.5 \text{ ergs/cm.}^2$$

BIBLIOGRAPHY

1. Van Houten, G.R.; Ceramic Bulletin, 38 (1959) 301.
2. Kingery, W.D.; J. Am. Ceram. Soc., 36 (1953) 362.
3. Williams, L.S. and Murray, P.; Metallurgia, 49 (1954) 210.
4. Bashforth, F. and Adams. S.C.; "An Attempt to Test the Theories of Capillarity", Cambridge University Press (1883).
5. Ellefson, B.S. and Taylor, N.W.; J. Am. Ceram. Soc., 21 (1938) 193.
6. Ellefson, B.S. and Taylor, N.W.; J. Am. Ceram. Soc., 21 (1938) 205.
7. Kingery, W.D. and Humenik, M.; J. Phys. Chem., 57 (1953) 359.
8. Adam, N.K.; "The Physics and Chemistry of Surfaces", Oxford University Press, London (1941).
9. Economos, G. and Kingery, W.D.; J. Am. Ceram. Soc., 36 (1953) 403.
10. Kingery, W.D. and Wygant, J.F.; Ceramic Bulletin, 31 (1952) 165; 31 (1952) 213; 31 (1952) 251; 31 (1952) 295; 31 (1952) 345; 31 (1952) 386.
11. Tripp, H.P. and King, B.W.; J. Amer. Ceram. Soc., 38 (1955) 432.
12. Allen, B.C. and Kingery, W.D.; A.I.M.E. Trans., 215 (1959) 31.
13. Kurkjian, C.R. and Kingery, W.D.; J. Phys. Chem., 60 (1956) 961.
14. Baxter, J.R. and Roberts, A.L.; "Symposium on Powder Metallurgy, 1954", The Iron and Steel Institute, London (1954).
15. Halden, F.A. and Kingery, W.D.; J. Phys. Chem., 59 (1955) 557.
16. Humenik, M. and Kingery, W.D.; J. Am. Ceram. Soc., 37 (1954) 18.
17. Kingery, W.D.; J. Am. Ceram. Soc., 37 (1954) 42.
18. Eremenko, W.N., Ivashchenko, Y.N., Nizhenko, V.I. and Fesenke, V.V.; Metallurgical Abstracts, 26 (1959) 149.
19. Kozakevitch, P. and Urbain, G.; J. Iron and Steel Institute, 186 (1957) 167.
20. Hauck, C.A.; Deadwyler, E.W. and Shelvin, T.S.; W.A.D.C. Technical Report 54-173, 2 (1956).
21. Knapp, W.J.; J. Am. Ceram. Soc., 36 (1953) 43.
22. Pincus, A.G.; J. Am. Ceram. Soc., 36 (1953) 152.

23. Jager, E. and Huttenlocher, H.; Ceramic Abstracts, 3 (1956) 64.
24. Kronberg, M.L.; Acta Metallurgical, 5 (1957) 507.
25. Hurlbut, C.S.; "Dana's Manual of Mineralogy", John Wiley and Sons Inc., London (1949).
26. Thilo, E., Jander, J. and Seemann, H.; Ceramic Abstracts, 11 (1958) 324.
27. Loftness, R.L.; U.S. Atomic Energy Commission Report NAA-SR-132, (1952).
28. Long, E.L. and Gray, R.J.; U.S. Atomic Energy Commission Report No. O.R.N.L. 2494 Metallurgy and Ceramics, (1958).
29. Metals Handbook Committee; "Metals Handbook", The Am. Soc. for Metals (1948).
30. Williams, J.C. and Nielsen, J.W.; J. Am. Ceram. Soc., 42 (1959) 229.
31. Baes, C.F. and Kellogg, H.H.; A.I.M.E. Trans., 197 (1953) 643.
32. Russell, A.S.; Alcoa Research Laboratories Technical Paper No. 10, (1956).
33. Bestul, A.B.; J. Am. Ceram. Soc., 42 (1959) 236.
34. Bewer, J.H.; Bureau of Standards, J. Research, 2 (1934).
35. Cullity, B.D.; "X-ray Diffraction", Adison Wesley (1956).
36. Donnay, J.D.H. and Harker, D.; Naturaliste Canadien, 67 (1940) 33.